Human memory CD8+ T-cells exhibit an intrinsic metabolic advantage as reflected by increased mitochondrial functionality and high glycolytic potential

---

Inauguraldissertation

zur

Erlangung der Würde eines Doktors der Philosophie

vorgelegt der

Philosophisch-Naturwissenschaftlichen Fakultät

der Universität Basel

von

Patrick Marc Gubser

aus Quarten-Oberterzen

Basel, 2013

Genehmigt von der Philosophisch-Naturwissenschaftlichen Fakultät auf Antrag der

Professoren:

Christoph Hess, Antonius Rolink und Ed Palmer

Basel, den 26.2.2013

Prof. Dr. Jörg Schibler

creative commons

Namensnennung-Keine kommerzielle Nutzung-Keine Bearbeitung 2.5 Schweiz

---

Sie dürfen:

das Werk vervielfältigen, verbreiten und öffentlich zugänglich machen

Zu den folgenden Bedingungen:

Namensnennung. Sie müssen den Namen des Autors/Rechteinhabers in der von ihm festgelegten Weise nennen (wodurch aber nicht der Eindruck entstehen darf, Sie oder die Nutzung des Werkes durch Sie würden entlohnt).

Keine kommerzielle Nutzung. Dieses Werk darf nicht für kommerzielle Zwecke verwendet werden.

Keine Bearbeitung. Dieses Werk darf nicht bearbeitet oder in anderer Weise verändert werden.

- Im Falle einer Verbreitung müssen Sie anderen die Lizenzbedingungen, unter welche dieses Werk fällt, mitteilen. Am Einfachsten ist es, einen Link auf diese Seite einzubinden.

- Jede der vorgenannten Bedingungen kann aufgehoben werden, sofern Sie die Einwilligung des Rechteinhabers dazu erhalten.

- Diese Lizenz lässt die Urheberpersönlichkeitsrechte unberührt.

Quelle: http://creativecommons.org/licenses/by-nc-nd/2.5/ch/   Datum: 3.4.2009

Table of Contents

SUMMARY

Intrinsic differences between naïve and memory CD8+ T-cells affect both quality and quantity of cognate antigen response. Cellular immune function and metabolic pathways are closely linked. The metabolic repertoire of naïve and memory T-cells remains largely unknown. Here we assessed key metabolic features of human naïve and effector-memory CD8+ T-cells under basal, metabolic stress, and activating conditions. Basal mitochondrial respiration was similar in both subsets. Memory cells, however, possessed more complex, tubular mitochondria, and displayed greater respiratory capacity and enhanced fatty acid oxidation. Basal glycolysis was also comparable in both subsets. Memory cells, however, showed an exclusive capacity to rapidly upregulate glycolysis after mitochondrial respiration blockage. In line with this finding, effector memory CD8+ T-cells expressed more cytoplasmic GAPDH levels with enhanced activity compared to naïve CD8+ T-cells.

Protective immunologic memory depends on antigen-experienced T-cells that are able to: (a) rapidly acquire effector function and (b) expand as secondary effector cells (Masopust and Picker, 2012). The clonal re-expansion of memory cells requires aerobic glycolysis (Warburg effect) in order to meet added biosynthetic and energetic demands (Vander Heiden et al., 2009). The metabolic requirements of rapidly responding effector memory CD8+ T-cells are unknown. Here we show that human effector memory CD8+ T-cells possess the intrinsic ability to upregulate aerobic glycolysis with unexpected rapid dynamics. In contrast to prototypical aerobic switch in activated T-cells, this early phase is insensitive to blockage of mTORC1, a known regulator of glucose metabolism in proliferating T-cells (Finlay et al., 2012; Fox et al., 2005). CD28 signaling via mTORC2 and AKT is required to sustain this early increased glycolyis. Importantly, preventing this early glycolytic phase by either blocking AKT activity or glucose deprivation, led to an impairment of IFN-γ secretion.

Therefore, increased metabolic capacities in effector memory CD8+ T-cells promote a primed state to immediately support high glycolytic activity upon activation. This early glycolytic phase is prerequisite for immediate effector function and therefore linking metabolic features with CD8+ T-cells recall functionality.

Our findings established differential metabolic repertoires between naïve and effector-memory CD8+ T-cells, with implications for strategies aiming to therapeutically manipulate CD8+ T-cell memory.

INTRODUCTION

Dynamics of the CD8+ T cell response

During acute viral infection, pathogen-specific naïve CD8+ T-cells become activated, followed by their rapid clonal expansion and differentiation into cytotoxic effector cells (Haring et al., 2006). Resolution of infection triggers the contraction of effector cells, which is accompanied by the formation of a long-lived memory pool (Cui and Kaech, 2010). Memory CD8+ T-cells provide a source of quiescent, antigen-experienced cells with high proliferative capacity (Geginat et al., 2003; Maus et al., 2004; Veiga-Fernandes et al., 2000) and a lower activation threshold than naïve cells (Adachi and Davis, 2011; Allam et al., 2009; Pihlgren et al., 1996) (**Figure 1**). These traits allow for a rapid generation of effector cells during secondary infection (Harty et al., 2000). The molecular basis defining T-cell memory remains an important unresolved issue in immunology.
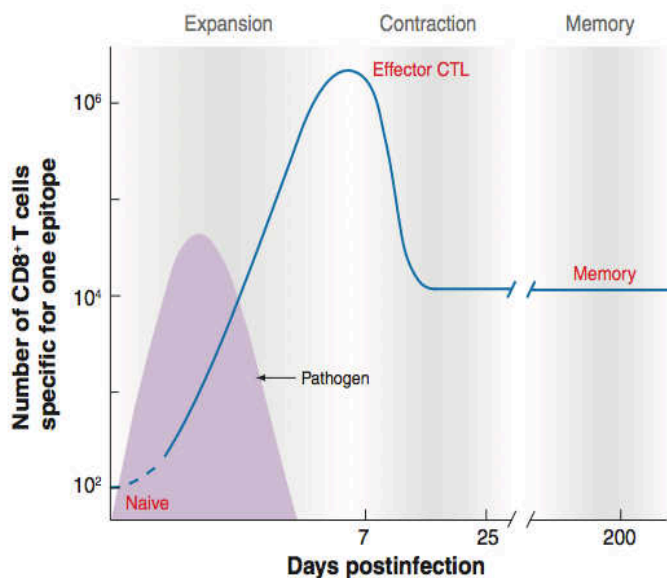
Figure 1. Number of antigen specific CD8+ T-cells in response to infection.

Antigen-specific CD8+ T-cell undergo massive expansion after an acute infection. In this expansion phase activated CD8+ T-cells acquire effector function with a subsequent differentiation into cytotoxic T lymphocytes (CTL). After clearance of the pathogen 90% to 95% of the effector T cells die during a contraction phase. The remaining 5–10% of the antigen-specific T-cells become the memory population.

picture modified from (Williams and Bevan, 2007)

Memory generation

"Cellular barcoding" revealed that a single naïve CD8+ T-cell can give rise both to effector and memory populations (Gerlach et al., 2010; Stemberger et al., 2007), raising the question, what influences the effector versus memory decision and in which phase memory is generated. The memory forming process is characterized by an increase of the IL7 receptor (CD127) and a downregulation of the effector marker KLRG1 (Buentke et al., 2006; Kaech et al., 2003; Sarkar et al., 2008; Schluns et al., 2000). The balance between the transcription factors T-bet and eomesodermin is coupled with the fate of CD8+ T-cells differentiating into effector or memory T-cells (Intlekofer et al., 2005). Various cytokines regulate expression of these transcription factors. The best understood of these is IL-12, where during the expansion phase it maintains high T-bet expression and drives effector generation (Joshi et al., 2007; Mescher et al., 2006; Pearce and Shen, 2007). In contrast, IL12 also inhibits eomesodermin which is thought to promote effector to memory transition (Takemoto et al., 2006). When inflammation subsides, IL12 levels decrease, promoting memory formation via increase of eomesodermin. Several studies have shown the importance of an efficient effector induction as an essential precondition for fully functional memory T-cells (Intlekofer et al., 2005; Xiao et al., 2009), however, other have demonstrated that memory formation can progress partly independent of effector cell differentiation (Joshi et al., 2007). Despite extensive studies in this area, conflicting memory T-cell differentiation models exist, a key difference being which phase of the immune response CD8+ memory is generated.

Memory CD8+ T-cells can be further divided into two main subsets which play distinct, but cooperative roles in protection of the host on a secondary challenge (Jameson and Masopust, 2009), the central memory (T cm) and the effector memory T-cells (T em) (Sallusto et al., 2004). Central-memory T-cells remain or re-express the lymph node homing markers CD62L and chemokine receptor 7 (CCR7). They are long lived cells that have a great potential to proliferate and a high capacity to produce IL2 upon antigen re-stimulation (Champagne et al., 2001). Due to their chemokine receptor pattern, central memory T-cells are located in secondary lymphoid organs and mainly excluded from non-lymphoid tissue sites such as skin or mucosa, where most pathogens are encountered.

In contrast, effector-memory (T em) cells lack CD62L and CCR7 expression but instead express chemokine receptors associated with homing to inflammatory sites such as CCR5 (**Figure 2**). This difference in migration pattern distributes effector memory CD8+ T-cells preferentially within non-lymphoid tissues or recirculating in peripheral blood. Effector memory T-cells are considered to have a more limited lifespan and a decreased proliferative potential compared to T cm and are therefore unlikely to significantly contribute during secondary clonal expansion (**Figure 3**). However, effector memory T-cells contain preformed cytotoxic granules to rapidly kill infected cells, and are poised to secrete high levels of effector cytokines such as IFN-γ and TNF-α (Hansen et al., 2009; Harari et al., 2009). In addition, their anatomical distribution in the non-lymphoid tissue places effector memory T-cells at pathogen entry sites where they able to utilize immediate effector functions. In line with this view, mouse studies have demonstrated that adoptively transferred CD8+ T em populations provide a greater degree of protection against a variety of infectious challenges than T cm, when measured early (within a few days) after challenge (Bachmann et al., 2005; Huster et al., 2006; Nolz and Harty, 2011). However, during re-exposure to virulent or chronic infections central memory T-cells are more efficient in controlling the pathogen (Nolz and Harty, 2011; Takemoto et al., 2006). During primary infections, when foreign antigen is quickly eliminated, maintenance of T cm is favored over

T em (Badovinac et al., 2007; Marzo et al., 2005; Wherry et al., 2003). More pathogenic

infections, longer antigen persistence or recurrent antigen exposure (as well as prime-boost

vaccinations) result in a higher number of T em (Masopust et al., 2006). Nevertheless,

differentiation factors that drive the generation of either effector- or central memory CD8+
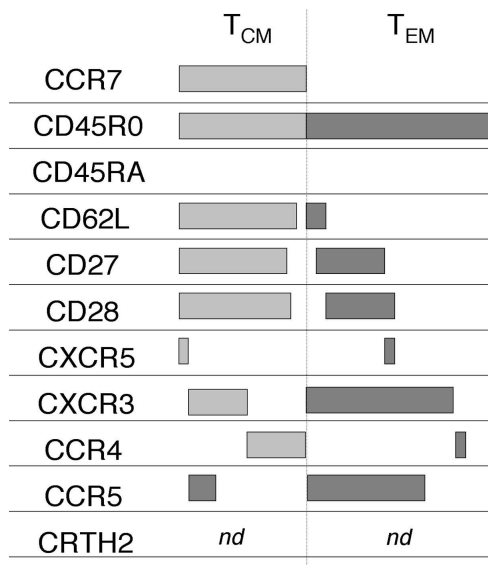
T-cells remain largely unknown.

Figure 2. Differential expression markers of central memory (Tcm) and effector memory (T em) T-cells

Central memory and effector memory CD8+ T-cells have different expression patterns of chemokine receptors. T cm are characterized by expression of the lymphnode homing receptors CCR7 and CD62L whereas T em lack expression of these markers.

picture modified from (Sallusto et al., 2004)

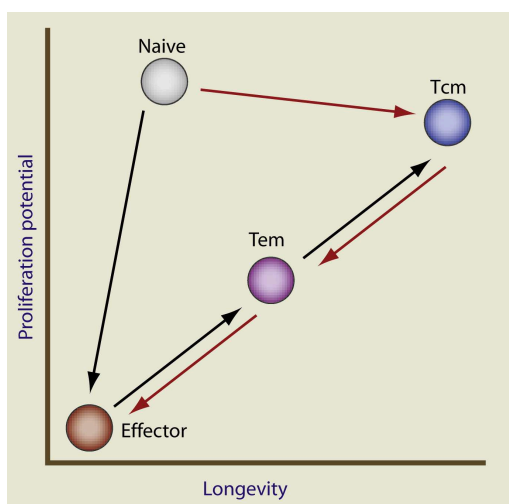

Figure 3. Proliferation potential and longevity of different CD8+ T-cell subsets

This simplified chart shows the longevity and the proliferation potential of naïve, effector and the two memory subsets: effector memory (Tem) and central memory (Tcm). The arrows between the subsets indicate the conflicting models of lineage differentiation.

chart modified from (Jameson and Masopust, 2009)

Metabolic changes in the life of a CD8+ T-cell

Access to sufficient nutrients is one of the most fundamental requirements for a cell to function normally in context of their specific function. This requirement can change drastically when a cell is stimulated to grow or proliferate. Nearly a century ago, Otto Warburg observed that cancer cells preferentially metabolized glucose to lactate than relying on the more energetically efficient mitochondrial oxidative pathways (Warburg, 1956). Studies on T-lymphocyte metabolism demonstrated similar findings. Whereas resting lymphocytes primarily use oxidative phosphorylation, activation leads to a shift towards glycolysis (Bental and Deutsch, 1993) (**Figure 3**). Since these cells used glycolysis in the presence of oxygen, this unique metabolic program was termed aerobic glycolysis (Warburg effect). This finding was surprising at that time since bioenergetically such a switch occurs in cases of altered mitochondrial function or in the absence of oxygen. A possible explanation for aerobic glycolyis might be a high demand for biomass. Cancer cells and activated T-cells both rapidly proliferate. Intermediates produced in the glycolytic pathway provide building blocks for biosynthesis of amino acids, nucleotides and lipids (Vander Heiden et al., 2009). It should be noted that increased glycolysis among effector cells is not only a prerequisite for growth and expansion, but also for acquisition of effector function (Cham and Gajewski, 2005a; Greiner et al., 1994; MacDonald, 1977). Blockade of this key metabolic pathway results in the diminution of efficacious CD8+ T-cell activation, clonal expansion and maturation (Cham et al., 2008; Macintyre et al., 2011; MacIver et al., 2011). In addition to the Warburg effect, CD8+ T-cell activation has been demonstrated to induce mitochondrial membrane hyper-polarization and to elicit mitochondrial biogenesis (D'Souza et al., 2007; Gergely et al., 2002). Inhibition of mitochondrial respiration attenuates CD8+ T-cell responses following viral challenge (Yi et al., 2006).

During effector-to-memory transition a reverse 'metabolic switch' occurs, where aerobic glycolysis is down modulated, again making OXPHOS the primary energy-generating pathway in the cell (Pearce et al., 2009).
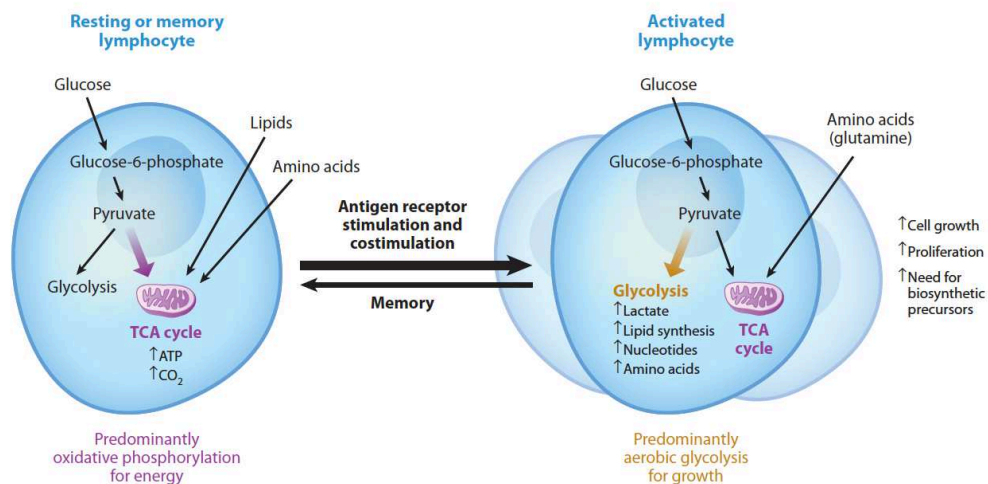
Figure 3. Metabolic changes in CD8+ T-cells upon activation.

Changes in metabolic signatures complements the functionality of CD8+ T-cells. Naïve CD8+ T-cells cells oxidize glucose-derived pyruvate, lipids and amino acids in the mitochondria resulting in a high ATP yield. Upon activation, glycolysis, as characterized by converting pyruvate to lactate, is increased. Simultaneously lipid oxidation is downregulated in order to prioritize biosynthesis over efficient ATP production. After the pathogen is cleared, memory formation in T cells is characterized by a metabolic switch back to oxidative phosphorylation, which results in an increased capacity for efficient energy generation.

picture from (Maciver et al., 2013)

mTOR integration of costimulatory signals and metabolism

In Drosophila, pathogen-associated molecular patterns (PAMPS) signal via Toll receptors, which leads to the production of the antimicrobial protein attacin (Tanji and Ip, 2005). In this system, antigen recognition and response are mediated via a single receptor. Development of the adaptive immune system with the stochastically rearranged, highly specialized antigen receptors made the immune response more complex. Ligation of the T-cell receptor (TCR) itself was no longer sufficient to decide what type of response should ensue. Additional instructions to orchestrate the immune response became necessary. For T–cells, accessory signals provides this information (Curtsinger and Mescher, 2010; Sharpe, 2009). Sensing the combination of antigenic and inflammatory signals by T-cells is crucial for a successful immune response. TCR stimulation (also referred as "signal1") on naïve CD8+ T-cells without co-stimulation ("signal2") promotes anergy. Particularly integration of CD28, as a co-stimulatory signal, is important for T-cells (Schwartz, 2003). Activation induced switch from oxidative phosphorylation to aerobic glycolysis in T-cells is also dependent on CD28 signaling (Cham and Gajewski, 2005b; Frauwirth et al., 2002b). This switch is not thought of as a consequence of T-cell, rather metabolic changes are an integral component of T-cell activation (Jones and Thompson, 2007). T-cells are able coordinate stimulatory signals ("signal1" and "signal2") with diverse additional environmental and metabolic cues ("signal3") through the highly evolutionary conserved mTOR pathway (Delgoffe and Powell, 2009; Mills and Jameson, 2009). Via mTOR (mammalian target of rapamycin), T-cells interpret these signals and are either activated or anergic, generate CD4+ effectors versus regulatory T-cells and generate CD8+ effectors or memory cells.

mTOR signaling

mTOR exist in two multiprotein complexes mTORC1 and mTORC2. In mammals mTOR is constituvely expressed and regulated post-translationally. mTORC1 is sensitive to immunosuppressive rapamycin whereas mTORC2 is mainly insensitive. Generally, growth factor or cytokine signaling leads to activation of phosphatidylinositide 3-kinases (PI3K) and to the subsequent generation of phosphatidylinositol 3-phosphate, which recruits AKT (also known as protein kinase B (PKB) and 3-phosphoinositide-dependent protein kinase-1 (PDK1) to the cell membrane. AKT gets phosphorylated by PDK1 at residue Thr308. Complete activation of AKT also needs phosphorylation at the carboxy-terminal Ser473 by mTORC2. AKT in turn, initiates the signaling cascade to activate mTORC1. In T-cells the PI3K-AKT-mTOR axis is activated by CD28 and IL2 (Colombetti et al., 2006). Additional important cytokine signaling via mTOR are IL7 and IL4 to prevent apoptosis in T-cells (Rathmell et al., 2001). IL12 and IFN-γ promote sustained activation of mTORC1 (Rao et al., 2010). mTORC1 activity is also profoundly regulated by amino acids, escpecially leucine (Proud, 2007). Amino deprivation or using the leucine antagonist N-acetyl-leucine-amide (NALA) decreased mTORC1 activity and T-cell function (Zheng et al., 2009). Working in opposition to the AKT/mTORC1 axis, the AMP-activated kinase (AMPK) complex promotes catabolic processes that maximize energy generation (Hardie, 2007). AMPK is activated by a decrease in the cellular ATP/AMP ratio and several other kinases including calcium/calmodulin-dependent protein kinase kinase 2 (CaMKK2) (Tamas et al., 2006). Targets downstream of mTORC1 are protein S6 kinases (S6Ks) and the translational repressor eIF4E-binding proteins (4E-BPs). Phosphorylation by mTORC1 promotes translation initiation and protein synthesis (**Figure 4**).
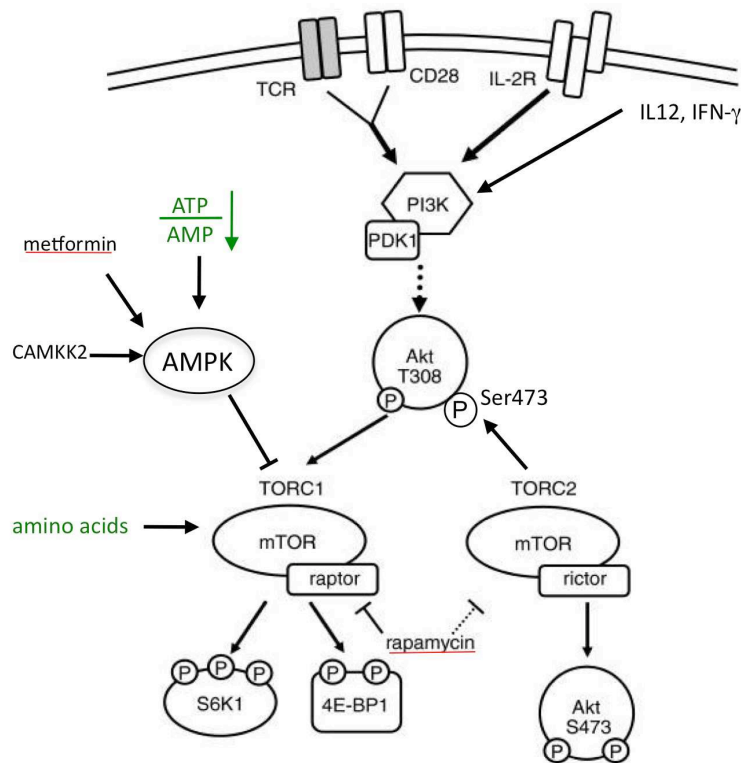
Figure 4. Activators of mTOR and its downstream targets.

This highly simplified chart shows mTOR signaling pathways in CD8+ T-cells. Immunological environmental cues are in black whereas metabolic inputs are indicated in green color. Drugs interfering with the signaling components are underlined with a red line.

scheme modified from (Delgoffe and Powell, 2009)

mTOR effects on CD4 T cell differentiation

At the metabolic level many is known for CD4+ TH1, TH2, TH17 and regulatory T-cells (T regs). Evidence for metabolic differences in these subsets came from studies dissecting the role of mTOR in T-cell differentiation. Treatment with rapamycin, an mTOR inhibitor, supressed CD4+ T-cell function and proliferation and promoted the differentiation into FOXP3+ T regs (Kopf et al., 2007; Zheng et al., 2007). In line with these findings, inhibiting mTORC1 via activation of AMPK with metformin, also led to an increase in Treg numbers (Michalek et al., 2011). Later studies dissected the individual contribution of the mTORC1 and mTORC2 complex for differential CD4 T-cell differentiation (Delgoffe et al., 2011). Taken together, a high mTOR activity in CD4+ T-cells leads to effector (Th1, TH2, TH17) differentiation, whereas low mTOR activity favours T reg generation (**Figure 5**).

mTOR effects on CD8+ T-cell

In CD8+ T-cells, mTOR facilitates anabolic processes during the expansion phase and therefore promote CD8+ effector generation, similar to CD4+ T cells (Intlekofer et al., 2005). However, effector subset differentiation in CD8+ T-cell is much simpler as compared to the CD4+ T-cells. Only one type of effector CD8+ T-cell is described: the cytotoxic T lymphocyte (CTL). Instead, activity of mTOR plays an important role in effector CTL versus memory differentiation. Surprisingly, mice that were infected with lymphocytic choriomeningits virus (LCMV) and treated with low doses of the mTOR inhibitor rapamycin during the expansion phase generated more CD8+ memory cells compared to untreated mice (Araki et al., 2009). Another independent study also confirmed this finding. In their study, IL12 led to an mTOR dependent upregulation of T-bet. Rapamycin decreased mTOR activity and led to a decrease in T-bet and a subsequent upregulation of eomesodermin (Rao et al., 2010). An increase in CD8+ T cell memory formation has also been reported by treatment with the AMPK activator metformin (Pearce et al., 2009). Together these studies

show interesting new strategies for modulation of the memory formation via metabolism

(**Figure 5**).
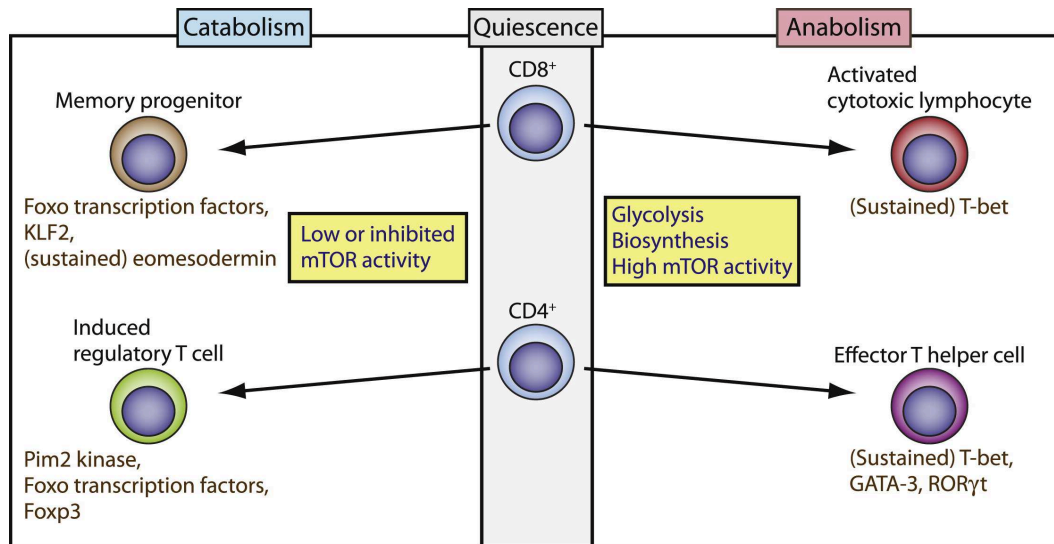
Figure 5. mTOR activity in the context of anabolic and catabolic processes.

High mTOR activity promotes anabolic processes and effector differentiation in both CD4+ and CD8+ T-cell subsets. This process is accompanied by increase in glycolysis and biosynthesis (right side). Low activity or inhibited mTOR activity leads to regulatory T-cell induction in CD4+ T-cells and memory formation in CD8+ T-cells (left side).

picture from (Powell and Delgoffe, 2010)

THESIS

The importance of metabolic regulation for normal immune function, differentiation and memory formation is well understood. However, despite the growing understanding on the interplay between metabolism and immune function, little interest has been put on the actual metabolic differences between the different established subsets. Given the fact that immune cells have to function in a broad variety of different environmental settings, they might also possess distinct metabolic repertoires. Likely, a T cell in the in the skin has to deal with very different nutrient conditions compared to a T cell in peripheral blood. At the site of an ongoing inflammation these differences might be even more pronounced. Memory T-cells have traditionally been characterized as metabolically quiescent cells, similar to their naïve counterparts. However, important qualitative differences exist between the responsiveness of naïve and memory CD8+ T-cells to activating signals and homeostatic cytokines (Cui and Kaech, 2010). Memory cells are known to have less stringent activation requirements (Rogers et al., 2000), are able to expand more rapidly following re-exposure to cognate antigen (Wherry et al., 2003) and have an increased production of effector molecules such as IFN-γ and TNF-alpha (Slifka and Whitton, 2000) compared to naïve T cells. It remains unknown whether these differences point to a divergence in the regulation of metabolic pathways between both subsets. We recently demonstrated that effector memory CD8+ T-cells have higher random motility compared to naïve CD8+ T-cells and produce more heat (Zenhaeusern et al., 2009), suggesting differences in their metabolic phenotype. Therefore we hypothesized that the *metabolic repertoire* is a defining feature of naïve vs. memory CD8+ T-cells.

EXPERIMENTAL PROCEDURES

Isolation of peripheral blood mononuclear cells and CD8+ T-cells

Blood samples were obtained from healthy donors after written informed consent. Peripheral blood mononuclear cells (PBMC) were isolated using standard density gradient centrifugation-protocols (LymphoprepTM, Fresenius Kabi, Oslo, Norway). CD8+ T-cells were either positively selected using MACS beads (Miltenyi Biotec GmbH, Bergisch-Gladbach, Germany) or negatively selected using the EasySep® Human CD8+ T-cell Enrichment Kit (Stemcell Technologies Inc., Vancouver, Canada).

Cell sorting

To isolate naïve and effector memory subsets, positively selected CD8+ T-cells were incubated with anti-CCR7 mAb-APC (FABP197, R&D systems Europe, United Kingdom) and with anti-CD45RA mAb-PB (clone 2H4, Beckman Coulter, California, USA). CCR7+CD45RA+ and CCR7^{neg}CD45RA^{neg} subsets were then sorted using the BD FACSVantage SE System (BD Bioscience, Mountain View CA, USA). A representative sort is shown in **suppl. Figure S1A-1C**. Sorted cells were rested for 3 hours in RPMI 1640 (Sigma-Aldrich, St. Louis, Missouri, USA), containing 10% human AB serum, 50 U/mL penicillin and 50 µg/mL streptomycin (all from Invitrogen, Carlsbad, California, USA), before continuing with downstream experiments.

Flow cytometry

For staining, cells were resuspended in FACS buffer (1% bovine serum albumin in PBS) and incubated with relevant antibodies for 30 min. in the dark at 4°C. To probe for mitochondrial mass, cells were stained with 100 nM mitotracker green (Invitrogen) and further processed according to the manufacturer's instructions. Data were acquired using a FACSCalibur flow cytometer (Becton Dickinson, Mountain View, CA, USA) and analyzed using FlowJo 8.8.7 software (Tree Star, Inc., Ashland, OR, USA).

Seahorse XF flux analyzer

The XF technology, introduced in 2006, combines an electro-optical instrument with plastic cartridges to enable the real-time measurement of cellular bioenergetics in a non-invasive, multi-well microplate format. Creating a transient micro-chamber of only 2 µl above the plated cells, the machine is able to measure small differences in the partial oxygen pressure and pH changes in an unbuffered culture medium. Changes in pH are proportional to the amount of lactic acid production and calculated as extracellular acidification rates (ECAR, mpH/min). The drop in oxygen partial pressure enables the instrument to calculate the oxygen consumption rate (OCR, pmoles/min). Four injection ports allow pharmacologic manipulation to interrogate different energetic states of the cells. Originally The XF24 flux analyzer was made for adherent cell cultures. Toxicologists, testing mitochondrial affection by pharmacological compounds, were the first users of this machine. Later different research areas (e.g. neurodegeneration, cancer, cell physiology) showed increasing interest in addressing mitochondrial dysregulation and respiratory capacity in various cell systems. Immunologists started using the XF technology in 2010 (Capasso et al., 2010) since the machine was not created to work with suspension cells as T lymphocytes. Additional coating of the wells with Cell-Tak (BD Bioscience), which is a bioadhesive extracted from the marine mussel Mytilus edulis, enables to use the Seahorse flux analyzer on lymphocytes.
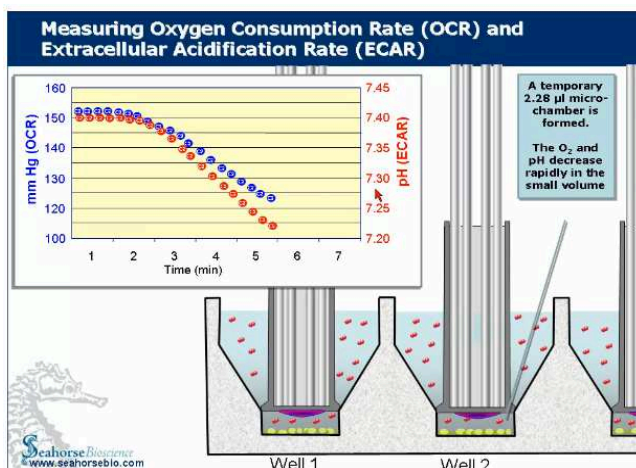

Figure 6. Measuring OCR and ECAR

The Seahorse XF24 flux analyzer is able to detect small decreases of pH and partial oxygen pressure in a temporally created micro-chamber. With these values oxygen consumption rate (OCR) and extracellular acidification rate (ECAR) are calculated in real time.

picture from Seahorse webinar, Seahorsebio webpage

OCR and ECAR measurements

To assess oxygen consumption rates (OCR, pmol/min) and extracellular acidification rates (ECAR, mpH/min) of CD8+ T-cell subsets, the Seahorse XF-24 metabolic extracellular flux analyzer was utilized (Seahorse Bioscience®, North Billerica, MA, USA). Briefly, CD8+ T-cell subsets were resuspended in serum-free unbuffered RPMI 1640 (Sigma-Aldrich) and plated onto Seahorse cell plates (6x10e5 cells/well) coated with Cell-Tak (BD Bioscience) to enhance T-cell attachment. Perturbation profiling of CD8+ T-cell metabolic pathway usage was performed by addition of oligomycin (1 µM), DNP (170 µM) and rotenone (1 µM) (all compounds from Sigma-Aldrich, St. Louis, Missouri, USA). Seahorse experiments were done using the following assay conditions: (2 min MIX TIME, 2 min WAIT TIME, and 4 to 5 min MEASURE TIME). Metabolic parameters were calculated as detailed in **Figure S2**.

Confocal microscopy

Experiments with live cells were performed using the 3I spinning disk confocal microscope (Intelligent Imaging Innovations, Denver CO, USA) with a 100x oil-immersion objective at 5% CO2 and 37⬚C (IMCF Facility, Biocenter, University of Basel). Cells were loaded with 50 nM 'mitotracker green' (MTG, Invitrogen) and 25 nM tetramethylrhodamine-ethyl-ester-perchlorate (TMRE, Invitrogen). Cells were incubated for 30 minutes with both dyes, washed and resuspended in fresh media. Since CD8+ T-cells are non-adherent cells, dye-loaded T-cells were allowed to settle onto culture slides (Ibidi, Munich, Germany) coated with poly-d-lysine for 20-30 minutes before imaging. Stacked images were then acquired at 0.5 µm intervals throughout the body of each cell.

Experiments with fixed cells were performed on an LSM 710 confocal microscope (Carl Zeiss, Jena, Germany) with a 100x oil-immersion objective. Fresh-sorted CD8+ T-cells subsets were allowed to attach by gravity on culture slides (BD Bioscience) coated with poly-d-lysine for 20 minutes. Attached cells were then fixed with 4% paraformaldehyde and permeabilized with 0.1% TritonX-100. Cells were stained with antibodies against FATP2 (Proteintech, Chicago IL, USA) and GAPDH (Cell Signaling Technology, Danvers MA,

USA), and labeled with the appropriate secondary antibodies. Stacked images were then collected 0.5 µm intervals. All images were processed using ImageJ (NIH).

Mitochondrial structural and functional analysis

Quantification of mitochondrial structure was carried out on cells labeled with MTG. Extraction of mitochondrial structural parameters was performed using a multi-step image-processing algorithm. Briefly, MTG intensities in raw images were enhanced by linear contrast stretch, spatially process using a 7x7 top hat filter to isolate mitochondrial objects and converted into a binary image by a threshold operation. Mitochondrial circularity (4π area/perimeter^2), length and form factor (1/circularity) were then calculated using ImageJ (NIH, Bethesda MD). Mitochondrial membrane potential ($\Delta\psi_m$) was calculated as the ratio of TMRE to MTG fluorescence intensities. MTG was included to normalize for mitochondrial mass differences between cell populations.

Electron microscopy

Transmission electron microscopy was performed at the Biocenter (University of Basel). Cells were sequentially fixed in 3% paraformaldehyde, 0.5% glutaraldehyde and 1% osmium tetraoxide, embedded and then cut into 60 nm sections. Micrographs (27'000x magnification) were obtained with a Morgagni 268 (FEI, Hillsboro OR, USA) transmission electron microscope operated at 80 kV. Image J software (NIH, Bethesda, USA) was used for measuring mitochondrial length (major axis) and width (minor axis). To quantify the morphology of mitochondria from both CD8+ T-cell subsets, the average aspect ratio was calculated (major axis to minor axis), an aspect ratio of 1 indicates a circular mitochondrial section.

Palmitate oxidation assay

To purify CCR7+ and CCR7^{neg} populations, CD8+ T-cells were isolated by negative selection and stained with anti-CCR7 mAb-PE (FABP197P, R&D Systems). To separate CCR7+ and CCR7^{neg} fractions, cells were incubated with anti-PE magnetic beads (Miltenyi Biotec GmbH), and sorted by positive selection using LD columns. The purity of CCR7+ and CCR7^{neg} cells after column isolation, assessed by flow cytometry, was always >80% (**Figure S3A-S3C**). Following isolation (using both sorting techniques), purified subsets were rested as described earlier. Palmitate oxidation among CD8+ T-cell subsets was assessed in unbuffered running media containing RPMI 1640-amino acid and RPMI 1640-vitamin solution (both from Sigma-Aldrich), supplemented with inorganic salts (according to the RPMI 1640 formulation) plus 2 mM glutamine. Sodium palmitate (P9767, Sigma-Aldrich) was complexed to fatty acid free BSA (ffBSA) (A6003, Sigma-Aldrich) and cells were resuspended in running media supplemented with 100 µM palmitate-ffBSA or (as control) 100 µM non-complexed ffBSA. The OCR of CD8+ T-cell subsets in the presence/absence of palmitate were recorded following the Seahorse protocol as described above.

Real time PCR

Total RNA was isolated using Trizol reagent (Invitrogen), and cDNA generated by GoScript reverse transcription system (Promega, Madison WI, USA). Real time PCR was performed using the Taqman technique (primer/probe sets from Applied Biosystems, Carlsbad CA, USA) with the 7900HT Real time PCR system (Applied Biosystems).

'In-Seahorse' T-cell activation

To monitor CD8+ T-cell activation inside the extracellular flux analyzer (i.e. in real time), αCD3 (clone HIT3a, Biolegend San Diego, CA, USA) and αCD28 (clone CD28.2, Biolegend) mAb were directly applied onto plated cells by using the instruments multi-injection ports. Different antibody concentrations were utilized according to the experiment. The doses for αCD3 and αCD28 are indicated in the figure legends for each experiment. Both antibodies were injected at 60 minutes after the experiment was initiated. ECAR and OCR of both subsets were recorded for the duration of the experiment (12 h). Mean acidification rates at pre- and post-antibody injection from 0-60 and 200-520 minutes, respectively, were used to describe the effects of both antibodies on CD8+ T-cell glycolysis. To control for non-specific effects of αCD3 mAb, experiments with isotype control mAb (IgG2aκ, Biolegend) were performed. For glucose-free Seahorse experiments unbuffered glucose free RPMI 1640 (Sigma-Aldrich) was used. For inhibitor experiments, LY294002, AKTi 1/2 (both from Sigma-Aldrich) and rapamycin (from Merck KGaA, Damrstadt, Deutschland) were injected 30-50 minutes prior to activation.

Immune blotting

Fresh-sorted cells were lysed in RIPA buffer (Thermo Scientific, Rockford IL, USA) and protein concentration determined by BCA protein assay kit (Thermo Scientific). Whole cell lysates were ran on 4-20% SDS page gels and transferred to nitrocellulose or PVDF membranes. Membranes were then probed with antibodies against HK1, LDHA, PKM2, PKM1/2, phospho-Akt (Thr308), phospho-Akt (S473), 4EBP1, p-4EBP1, and GAPDH (all from Cell Signaling Tech.), OGDH (Proteintech) and PDK1 (Abcam, Cambridge, UK). The blots were then stained with the appropriate secondary antibody. The Odyssey imaging system (LICOR, Lincoln NE, USA) was used for detection.

Glucose uptake

Sorted CD8+ T-cell subsets were incubated with a combination of αCD3 and αCD28 mAb (as indicated) for 45 minutes in serum free RPMI 1640, in the presence of 50 μM 2-NBDG (Invitrogen). Non-stimulated cells were included as controls. The cells were then washed, and NBDG uptake assessed using a Cyan-ADP Flow Cytometer (Beckman Coulter, Brea, California, USA).

GAPDH activity

To assess GAPDH activity in CD8+ T-cells, a GAPDH assay kit from Innoprot (Innoprot, Zitek-Mintegia, Spain) was utilized. Fresh-sorted naïve and EM cells (5x10e5 cells per subset) were processed according to the manufacturer's instructions.

Lactate measurements

Fresh sorted cells were seeded into U-bottom 96-well plates (2.4x10e5 cells/well) in glucose free RPMI1640 (Invitrogen). Each well was supplemented with glucose and inhibitors as indicated and activated with soluble αCD3 (2 μg/mL) and αCD28 (20 μg/mL) mAbs. Non-stimulated cells were included as controls. Lactate levels were measured using the Lactate Assay Kit from BioVision (BioVision, Inc., San Francisco, USA).

Proliferation

Sorted cells were labeled with the cell proliferation dye eFluor670 (eBioscience, San Diego, CA, USA) at a final concentration of 2.5 μM and seeded into a U-bottom 96 well plate (1.7x10e5 cells/well). The plated cells were then activated with αCD3 (2 μg/mL) and αCD28 (20 μg/mL) mAb in serum free RPMI1640. AB serum was then added 3h after activation. Proliferation was measured 3 days post-activation by flow cytometry.

IFN-γ ELISA

Sorted cells were plated into U-bottom 96 well plates (3x10e5 cells/well) using glucose free RPMI medium. For kinase inhibitor experiments, cells were cultured in 10 mM glucose then treated with LY294002 (10 µM), AKTi 1/2 (10 µM) and rapamycin (20 ng/ml). For glucose dependency experiments, plated cells were treated with 10 mM glucose or 10 mM 2-deoxy-D-glucose (**see also Figure 21**). The treated cells were then activated with αCD3 (2 µg/mL) and αCD28 (20 µg/mL) and AB serum was added 3 hours later. Human IFN-γ levels were measured in supernatants at 12 hours post-activation using a High Sensitivity IFN-γ ELISA kit (eBioscience).

CD69 expression

Isolated CD8+ T-cells were incubated with anti-CCR7 mAb-APC (FABP197, R&D systems Europe, United Kingdom) and with anti-CD45RA mAb-PB (clone 2H4, Beckman Coulter, California, USA). The same culture conditions as for the IFN-γ ELISA have been used. At 8 hours post-activation, the cells were stained with anti-CD69 mAb-PE (FN50) and the appropriate isotype control mAb (both from ImmunoTools Gmb, Friesoythe, Germany). By gating on the two subpopulations CD69 upregulation has been measured in T naïve and T effector memory cells.

Statistical analysis

Data were assessed using either paired Student t-tests (two-sided) or Man Whitney tests. Values of $p < 0.05$ were considered to be statistically significant. For comparison of increases (pre/post) in paired samples a linear regression model was used.

RESULTS

Naïve and effector memory CD8+ T-cell populations display distinct oxidative capacities

Aiming to delineate the metabolic signature of quiescent naïve and antigen-experienced CD8+ T-cell subsets, fresh isolated cells were sorted into CD45RA+CCR7+ (naïve, NV) and CD45RA^{neg}CCR7^{neg} (effector memory, EM) subpopulations (**Figure S1A-S1C**). This sorting strategy has been extensively utilized to investigate functional differences between naïve and antigen experienced CD8+ T-cells (Geginat et al., 2003; Romero et al., 2007; Tomiyama et al., 2002). The oxygen consumption rate (OCR) of both cell populations under basal and chemically induced metabolic stress-conditions was measured by utilizing a metabolic extracellular flux analyzer (**Figure 7A**). Mitochondrial stress was induced by addition of oligomycin (ATP synthase blocker), DNP (mitochondrial uncoupler), and rotenone (Complex I inhibitor). All measurements were made in serum free, unbuffered standard RPMI, containing glucose (11 mM) and glutamine (2 mM) as the major fuel sources. The obtained respiratory profile provides basal OCR, ATP-coupled respiration, maximal/spare mitochondrial capacity, leak respiration and non-mitochondrial respiration (detailed in **Figure S2A**).

Basal OCR was comparable between naïve and effector memory populations (mean NV vs. EM: 50 and 60 pMol/min, respectively, n=6, p=0.33) (**Figure 7B**). This indicates that in the presence of glucose and glutamine and in the absence of serum, the rate of mitochondrial substrate oxidation is comparable between quiescent naïve and effector memory CD8+ T-cell subsets. In agreement with this finding, there was no measurable difference in ATP-coupled respiration (mean NV vs. EM: 36 and 48 pMol/min, respectively, n=6, p=0.23) (**Figure 7C**) and leak respiration (mean NV vs. EM: 14 and 12 pMol/min, respectively, n=6, p=0.49) (**Figure 7D**) between naïve and effector memory CD8+ T-cells. In addition, there was no significant difference in non-mitochondrial respiration between naïve and effector memory CD8+ T-cell
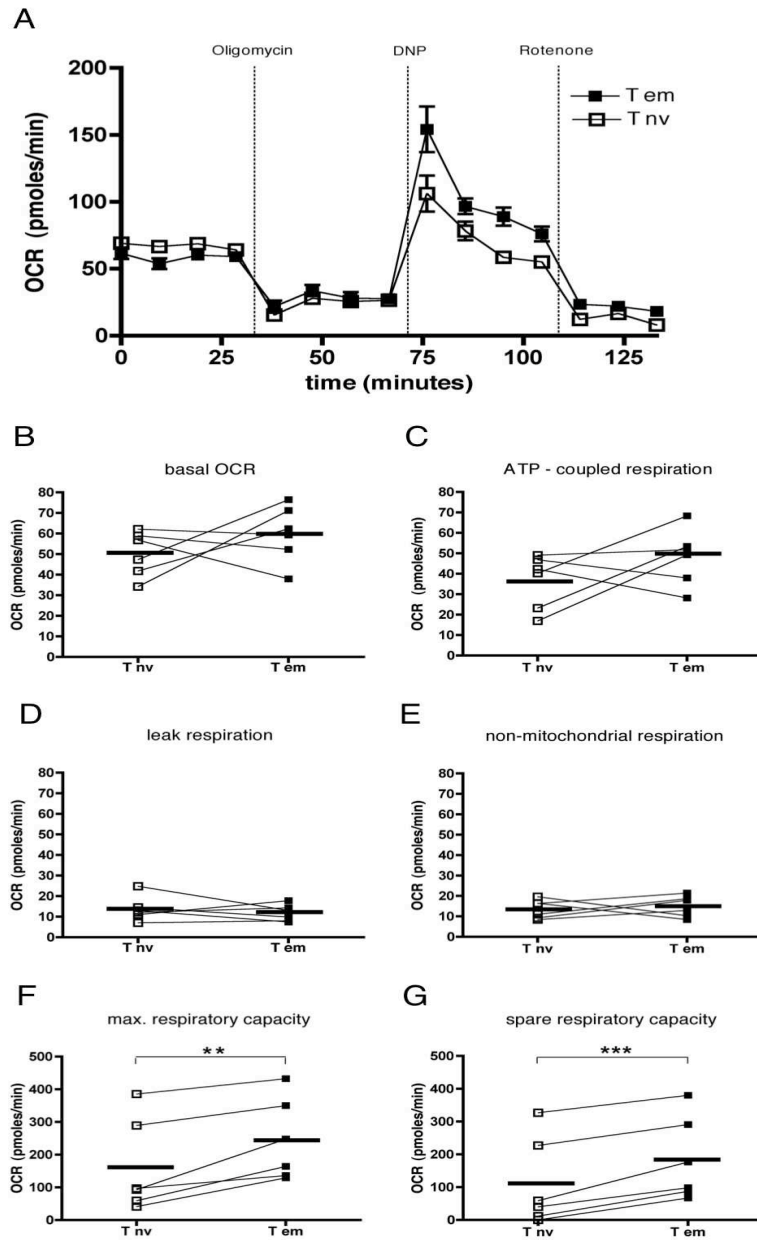
Figure 7. Mitochondrial respiration-signature of effector memory vs. naïve CD8+ T-cells.

(**A**) Representative oxygen consumption rate (OCR) graph of human naïve (□) and effector memory (■) CD8+ T-cells cultured in glucose/glutamine containing unbuffered RPMI. The OCR of fresh-sorted CD8+ T-cell subsets was monitored in real-time using the Seahorse extracellular flux analyzer under basal conditions, and following perturbation of mitochondrial function with oligomycin (ATP synthase blocker), DNP (mitochondrial uncoupler), and rotenone (Complex I inhibitor).

(**B**-**G**) Key respiratory parameters were calculated following perturbation of mitochondrial function with oligomycin, DNP, and rotenone. Graphs show basal respiration (**B**), ATP-coupled respiration (**C**), leak respiration (**D**), non-mitochondrial respiration (**E**), maximal respiratory capacity (**F**), and spare respiratory capacity (**G**) of naïve (□) and effector memory (■) CD8+ T-cells. Pooled paired data and mean values from 6 independent experiments/donors are shown. ** indicates $p=0.006$, *** indicates $p<0.001$ (paired Student t-test).

See also **supplementary Figure S1A-S1C**, **S2A**

subsets (mean NV vs. EM: 14 and 15 pMol/min, respectively, n=6, p=0.68) (**Figure 7E**). Maximal respiratory capacity, however, was consistently increased in effector memory CD8+ T-cells compared to naïve cells (mean NV vs. EM: 160 and 243 pMol/min, respectively, n=6, p=0.006) (**Figure 7F**). This increased respiratory capacity was only observed following uncoupling of mitochondrial proton motive force with DNP, signifying that effector memory CD8+ T-cells possess a higher spare respiratory capacity (SRC) than naïve cells (mean NV vs. EM: 111 vs. 183 pMol/min, respectively, n=6, p<0.001) (**Figure 7G**). In agreement with this finding, an increased SRC has recently been described as a key component of murine CD8+ T-cell memory formation (van der Windt et al., 2012). Differences in ATP turnover could explain the disparity in mitochondrial respiratory capacity between CD8+ T-cell subsets (Zenhaeusern et al., 2009). Using the above parameters, we calculated the cellular respiratory control (CRC) ratio, which is an estimate of mitochondrial functionality independent of ATP turnover (Brand and Nicholls, 2011). It is the ratio of the uncoupled respiratory rate [state 3U, $OCR_{peak-DNP}$] and the respiratory rate following addition of oligomycin [state 4O, $OCR_{oligomycin}$]. Effector memory CD8+ T-cells displayed a higher CRC ratio than naïve cells (mean NV vs. EM: 12 and 21, n=6, p=0.049), indicating that the observed difference in respiratory capacity is independent of the rate of ATP utilization by both subsets.

Naïve and memory CD8+ T-cells display disparate mitochondrial phenotypes

Higher maximal respiratory capacity among memory CD8+ T-cells suggests that mitochondrial biogenesis is a requirement for cells differentiating from a naïve to a memory phenotype. Congruent with the increased SRC, mitochondrial mass of murine memory T-cells were recently shown to be greater than that of their naïve counterparts (van der Windt et al., 2012). Comparing the mean fluorescence intensity of naïve and effector memory CD8+ T-cells loaded with the non-voltage dependent fluorescent mitochondrial dye mitotracker green (MTG), we also observed higher mitochondrial mass in human effector memory CD8+ T-cells (**Figure 8A**). Interestingly, effector memory cells consisted of two distinct populations, MTG^{dim} and MTG^{bright}, whereas naïve cells were primarily MTG^{dim}. Next, we characterized the morphology of mitochondria in naïve and effector memory CD8+ T-cell subsets. Fresh-sorted naïve and effector memory CD8+ T-cells were loaded with MTG, and mitochondrial morphology assessed by live-cell confocal microscopy. Images were then processed by well-established spatial filtering techniques (Hom et al., 2011; Koopman et al., 2006). Effector memory CD8+ T-cells were consistently found to possess mitochondria that were tubular in morphology, whereas naïve CD8+ T-cells had shorter, fragmented mitochondria (**Figure 8B**). Morphometric quantification demonstrated that mitochondria with longer branch length are present at higher frequency in effector memory CD8+ T-cells than in naïve counterparts (median mitochondrial branch length of NV vs. EM: 0.88 vs. 1.07 µm, respectively, p<0.0001) (**Figure 8C**). Additionally, mitochondria with an increased 'form factor' (a measure of mitochondrial complexity) (Hom et al., 2011), were detected at higher frequency in effector memory CD8+ T-cell than in naïve cells, indicating that mitochondria in effector memory cells are more interconnected than their naïve counterparts (mean 'form factor' of NV vs. EM: 1.2 and 1.4, respectively, p=0.005) (**Figure 8D**). CD8+ T-cell mitochondrial morphology was further assessed by transmission electron microscopy. Mitochondria in naïve CD8+ T-cells were predominantly short, bean shaped with sparse cristae connectivity and an expanded
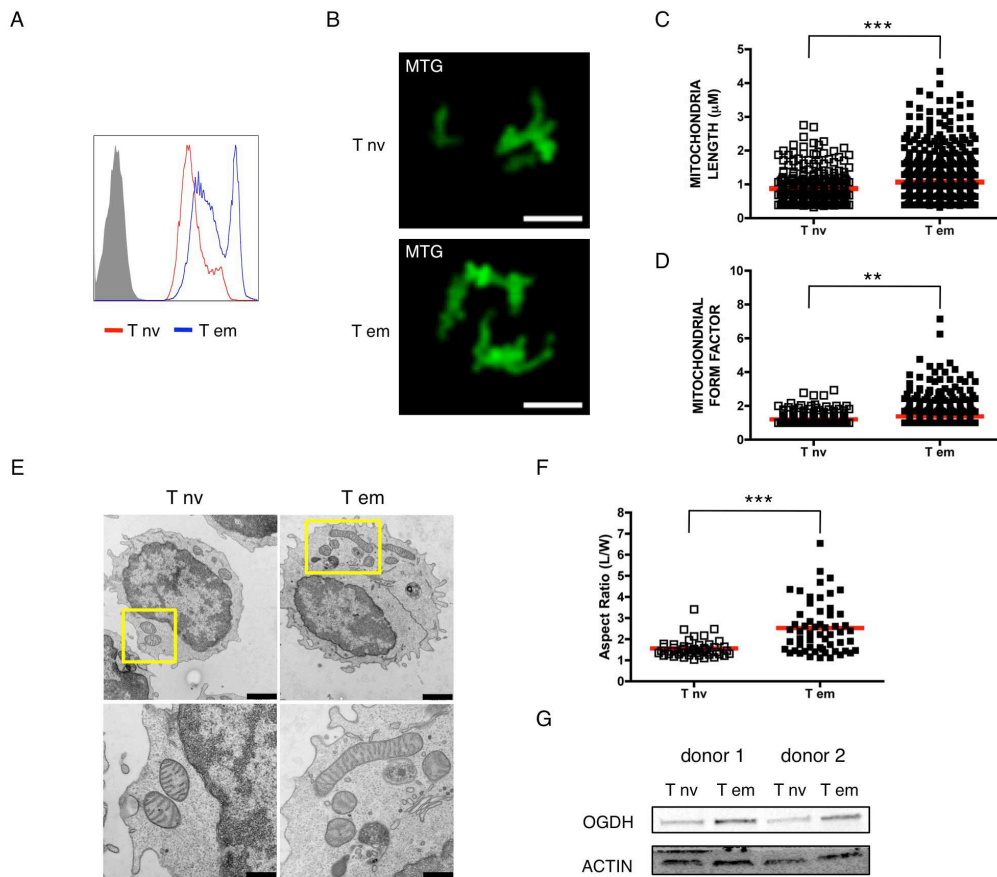
Figure 8. Mitochondrial mass and morphology of effector memory vs. naïve CD8+ T-cells.

(**A**) Histogram comparing 'mitotracker green' (MTG)-loaded naïve and effector memory CD8+ T-cells (representative of n=3 independently assessed donors). Filled gray histogram shows unstained control.

(**B**) Stacked confocal microscopy images of MTG loaded naïve and effector memory CD8+ T-cells. Live cell images were collected by spinning disk confocal microscopy using the Z-stack function of the microscope (24 sections, 0.5 µm between sections) and processed for morphometric analysis. Magnification = x100, scale bars = 3 µm.

(**C**, **D**) Measurements of mitochondrial length (C) and 'form factor' (D) among naïve and effector memory CD8+ T-cells. Both parameters were quantified from morphometrically processed live cell images. One of three independent experiments is shown, with 20-40 cells analyzed per experiment. Data are depicted as scatter plots. ** indicates p=0.005, *** indicates p<0.0001 (Mann-Whitney test).

(**E**) Transmission electron micrographs (magnification = x28'000) of naïve and effector memory CD8+ T-cells. Yellow squares in the top panel mark inset images shown in the bottom panel. Scale bars = 1000 nm (top), 500 nm (bottom).

(**F**) Summary of mitochondrial aspect ratio (length of major axis to minor axis) derived from transmission electron micrographs. 1 of 3 independent experiments is shown, with 10 cells analyzed per experiment. Data are depicted as scatter plots. *** indicates p=0.0001 (Mann-Whitney test).

(**G**) Immunoblot analysis of oxoglutarate dehydrogenase (OGDH) expression among naïve and effector memory CD8+ T-cells. Actin was used as loading control. Results from 2 of 3 independently assessed donors are shown.

matrix volume (**Figure 8E**, left panels). In contrast, mitochondria in effector memory CD8+ T-cells had long, ribbon like mitochondria with more laminated cristae and more compact matrix volume (**Figure 8E**, right panels). Morphometric analyses of electron microscopy images (aspect ratio= major axis to minor axis length) also captured disparities in the morphology of mitochondria between naïve and effector memory CD8+ T-cells. Similar to the finding above, mitochondria of effector memory CD8+ T-cells displayed longer, tubular mitochondria, whereas mitochondria of naïve cells had a more rounded morphology (mean aspect ratio of N vs. EM: 1.6 and 2.5, respectively, p=0.0001) (**Figure 8F**).

Given the difference in mitochondrial mass between CD8+ T-cell subsets, we probed for the expression of oxoglutarate dehydrogenase (OGDH), a key enzyme in the Kreb's cycle, as a marker for differences in mitochondrial content. In keeping with the functional and mass differences described above, OGDH protein was expressed at higher levels in effector memory CD8+ T-cells (**Figure 8G**).
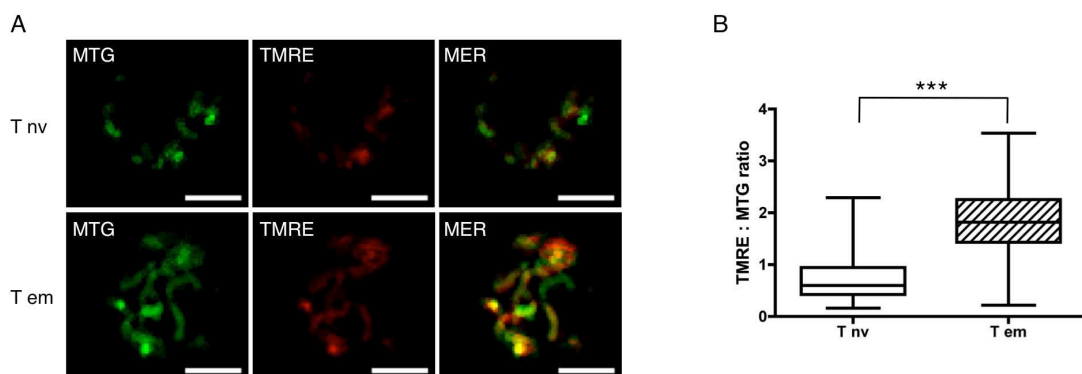
Figure 9. Mitochondrial membrane potential of effector memory vs. naïve CD8+ T-cells.

(**A**) Stacked confocal images of MTG and tetramethylrhodamine-ethyl-ester-perchlorate (TMRE) loaded CD8+ T-cells. Shown are single channel and merged (MER) images of naïve and effector memory cells loaded with both dyes. Magnification = x100, scale bars = 3 µm.

(**B**) Mitochondrial membrane potential of fresh isolated CD8+ T-cells was determined by normalizing TMRE intensity to MTG. One of three independent experiments is shown. The data are depicted as a box and whiskers plot, summarizing data from n=44 naïve, and n=25 effector memory CD8+ T-cells. *** indicates $p < 0.0001$ (Mann-Whitney test).

Lastly, we probed for the functio nal status of CD8+ T-cell mitochondria by measuring the mitochondrial membrane potential ($\Delta\psi_m$) of both subsets via live-cell imaging. Fresh-sorted cells were loaded with TMRE (a voltage dependent dye) and MTG, and mitochondrial membrane potential was calculated using the fluorescence intensity ratio of both dyes (TMRE to MTG) (**Figure 9A**). MTG was utilized to correct for differences in mitochondrial mass between cell types (Hom et al., 2011). Mitochondrial membrane potential was lower in naïve CD8+ T-cells compared to effector memory counterparts (**Figure 9B**), indicating, that in addition to mass differences, mitochondria of effector memory cells also possess greater functional activity than those of naïve cells. Together these results demonstrate that the mitochondrial mass, shape, connectivity and functionality are distinct between naïve and effector memory CD8+ T-cells.

Fatty acid metabolism is enhanced in memory CD8+ T-cells compared to naïve cells

It was previously demonstrated that fatty acid oxidation (FAO) is enhanced in mouse CD8+ T-cells during effector to memory differentiation (Pearce et al., 2009). It is not known, however, whether differences in FAO exist between quiescent human naïve and memory CD8+ T-cell subsets. To begin to test for such differences, CD8+ T-cells were sorted into CCR7+ and CCR7^{neg} fractions (**Figure S3**). This simplified sorting strategy yields a CCR7+ population highly enriched for naïve cells, and a CCR7^{neg} effector memory population containing both CD45RA re-expressing and CD45RA^{neg} cells. This strategy was used exclusively for FAO experiments in order to minimize time that cells are cultured *ex vivo*. Oxygen consumption was monitored using an in-house media (glucose free, unbuffered) in the presence or absence of palmitate complexed to ffBSA (100 µM). In the presence of palmitate-ffBSA there was a marked increase in the basal OCR of effector memory CD8+ T-cells, compared to control cells exposed to ffBSA (mean increase: 18 pMol/min, n=9, p<0.005, **Figure 10A**, right panel), whereas only a modest, statistically non-significant increase in basal OCR was observed in naïve-enriched cells exposed to palmitate-ffBSA (mean increase: 3 pMol/min, n=9, p=0.49, **Figure 10A**, left panel). A paired-ratio analysis of both OCR ratios (OCR palmitate to OCR control) was used to compare palmitate induced FAO between quiescent CCR7+ (naïve-enriched) and CCR7^{neg} effector memory subsets. The mean OCR ratio was significantly higher in effector memory cells (regression test, p=0.007, **Figure 10B**). This suggests that, although FAO occurs in both quiescent populations, the capacity to utilize fatty acids as a substrate for energy metabolism is greater in effector memory CD8+ T-cells. Under glucose free conditions, with glutamine being the primary energy source via glutaminolysis, basal OCR of naïve and effector memory T-cells were similar (**Figure S4**). Thus, increased FAO by effector memory CD8+ T-cells is not related to intrinsic differences in basal energy demands between subsets.
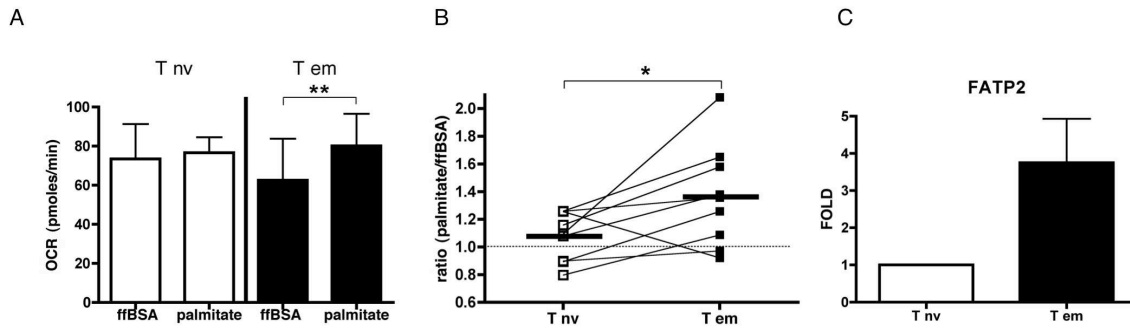
Figure 10. Fatty acid oxidation by naïve and effector memory CD8+ T-cells.

(**A**) Analysis of palmitate induced respiration (fatty acid oxidation) by quiescent CD8+ T-cell subsets. OCR of naïve-enriched (□) and effector memory (■) CD8+ T-cells from n=9 donors were measured by using the extracellular flux analyzer, culturing cells either with fatty acid free BSA (ffBSA) or with 100 µM palmitate-ffBSA. Data are presented as bar graphs ± SD. ** indicates p=0.004 (paired Student t-test).

(**B**) Paired ratio analysis of palmitate-induced respiration of naïve(-enriched) (□) and effector memory (■) CD8+ T-cells. The ratio of 'palmitate OCR' to 'ffBSA OCR' for paired subsets was used to compare palmitate oxidation between both populations. Data and mean values from n=9 donors are shown. A generalized linear model was used to calculate an interaction p-value between the two variables. * indicates p=0.007.

(**C**) Relative FATP2 expression between naïve (□) and effector memory (■) CD8+ T-cells. Both transcripts were normalized to actin mRNA levels (n=3 donors, ±SD).

Given these functional differences, we next probed for differences in the expression of genes involved in fatty acid metabolism in both cell types using a PCR based array. Genes differentially expressed in effector memory CD8+ T-cells compared to naïve CD8+ T-cells (**Figure S5**) were confirmed by real time PCR. The gene encoding fatty acid transporter 2 (FATP2) was most prominently upregulated in effector memory CD8+ T-cells (**Figure 10C**). FATP2 has two established functions in fatty acid metabolism. First, it enhances the uptake of long chain/very long chain free fatty acids, and second it activates free fatty acids via its acyl-CoA synthetase activity (Falcon et al., 2010). We probed for FATP2 protein expression by confocal microscopy in both CD8+ T-cell subsets. In line with differential expression at the mRNA level, FATP2 protein expression was greater in effector memory than in naïve CD8+ T-cells (**Figure 11A and 11B**). Moreover, FATP2 localization in naïve CD8+ T-cells was concentrated in small, primarily perinuclear compartments

33

(**Figure 11A, panels 1-3**), whereas in effector memory CD8+ T-cells localization was in larger cytoplasmic compartments (**Figure 11B, panels 1-3**). In all, these functional and cell-biologic findings suggest that, although FAO is utilized in both subsets, greater built-in capacity for FAO is characteristic of effector memory CD8+ T-cells.
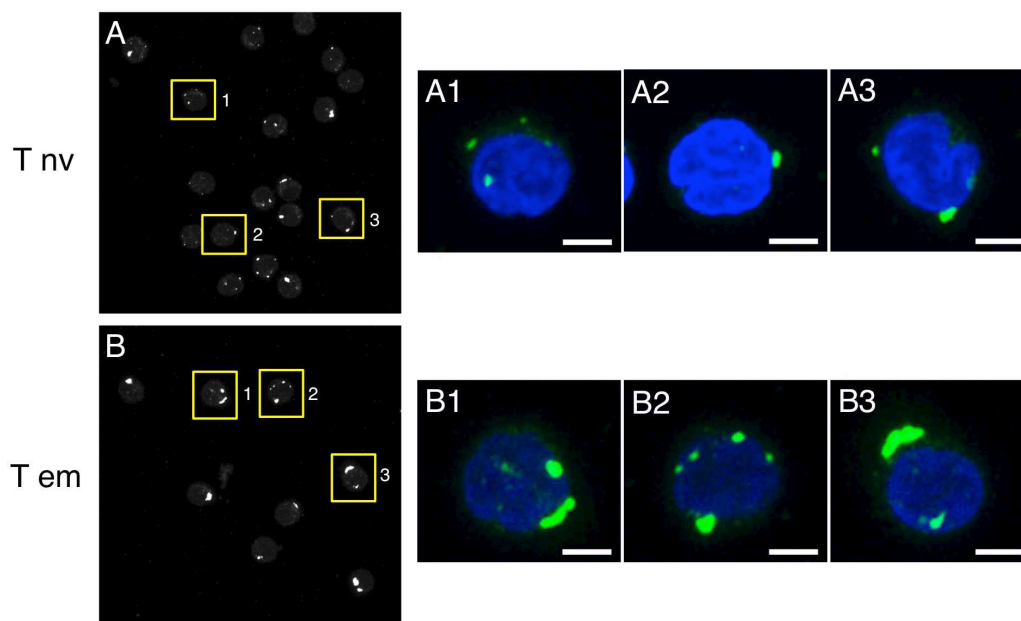

Figure 11. FATP2 expression by naïve and effector memory CD8+ T-cells.

(**A**, **B**) Stacked confocal microscopy images of (**A**) naïve and (**B**) effector memory CD8+ T-cells stained with anti-FATP2 mAb (green), counterstained with DAPI (blue; nucleus). Yellow boxes mark inset images shown in A1-3 and B1-3. Representative of n=3 independently assessed donors. Magnification = x100, scale bars = 3 μm.

See also **supplementary Figure S3A-S3C**, **S4 and S5**

Quiescent naïve and effector memory CD8+ T-cells display distinct glycolytic capacities

Mitochondrial respiration is the major ATP source for resting lymphocytes (Plas et al., 2002; Rathmell et al., 2000). How readily aerobic glycolysis can be utilized among quiescent naïve and memory CD8+ T-cells is not known. By measuring the extracellular acidification rate (ECAR) at basal conditions and following drug-induced modification of mitochondrial respiration (oligomycin, DNP, and rotenone; detailed in **Figure S2B**), we determined the glycolytic potential of naïve and effector memory CD8+ T-cells. The basal ECAR was similar for naïve and effector memory CD8+ T-cells (mean N vs. EM: 0.97 and 1.58 mpH/min, respectively, n=6, p=0.12) (**Figure 12A and 12B**). However, following inhibition of mitochondrial respiration, the ECAR of effector memory CD8+ T-cells rapidly increased to a mean of 4.73 mpH/min, whereas naïve CD8+ T-cells maintained their glycolytic rate at a mean of 1.82 mpH/min (n=6, p=0.009) (**Figure 12A, 12C**). The viability of both subsets, as determined by 7-AAD staining, was similar following treatment with all three compounds (data not shown), indicating that the inability of naïve T-cells to upregulate glycolysis is not due to a selective decrease in viability of this subpopulation.
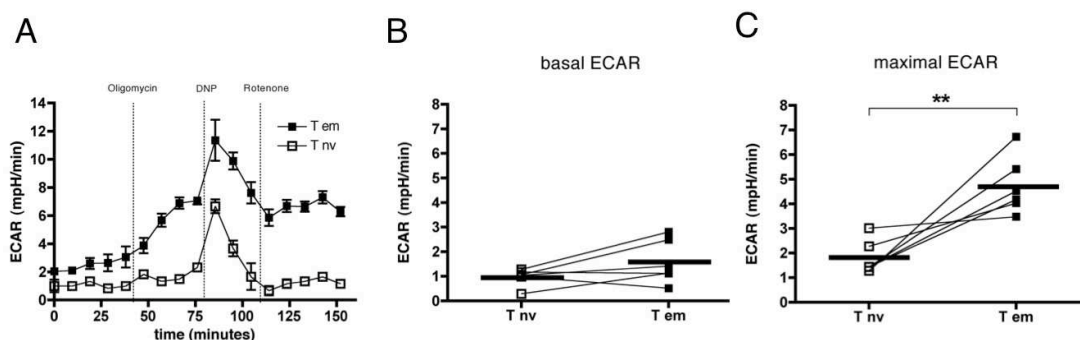

Figure 12. Glycolytic potential of naïve and effector memory CD8+ T-cells.

(**A**) Representative extracellular acidification rate (ECAR) graph of naïve (□) and effector memory (■) CD8+ T-cells. The ECAR of fresh-sorted CD8+ T-cell subsets was monitored in glucose/glutamine containing media.

(**B**, **C**) ECAR of naïve and effector memory cells were assessed under basal conditions (**B**), and following inhibition of mitochondrial respiration with oligomycin, DNP and rotenone (**C**). Pooled paired data and mean values from 6 independent experiments/donors are shown. ** indicates p=0.009 (paired Student t-test).

Regulation of glycolytic activity in naïve and effector memory CD8+ T-cells

We hypothesized that disparate glycolytic capacity of naïve vs. effector memory CD8+ T-cells following activation could be related to either differential availability of enzymes involved in glycolytic flux and/or a subset-specific capacity to increase glucose uptake following activation. To address the former, we probed for the expression of key enzymes along the glycolytic pathway by immunoblotting. Hexokinase 1 (HK1), glyceraldehyde-3-phosphate dehydrogenase (GAPDH), pyruvate kinase M2 (PKM2), and lactate dehydrogenase A (LDHA) were all comparably expressed in naïve and effector memory CD8+ T-cells, indicating that the glycolytic machinery is present in both subsets (**Figure 13A**). To determine whether CD8+ T-cell activation induces early subset specific increase in glycolytic enzymes, naïve and effector memory cells were stimulated with αCD3 (10μg/mL) and αCD28 (20μg/mL) mAb for 3 hours, and enzyme expression-levels were again assessed by immunoblotting. GAPDH, LDHA, HK1, PKM1/2, and PKM2 expression levels remained similar under non-stimulated and stimulated conditions, indicating that the observed increase in glycolysis is not due to upregulation of these enzymes (**Figure S7**). Glucose metabolism is a net product of glycolytic and gluconeogenic pathway activity. Therefore, transcript levels of fructose-1,6-bisphosphatase-1 (FBP1), a key enzyme of gluconeogenesis, were also assessed. Intriguingly, transcripts of FBP1 were markedly reduced in effector memory CD8+ T-cells (**Figure 13B**). This finding suggests that glucose flux in naïve cells can be shunted from fructose 1,6 bisphosphate back to fructose 6-phosphate, thus decreasing net glucose utilization along the glycolytic pathway.

Given that key glycolytic enzymes were present at similar levels in naïve and effector memory CD8+ T-cells, we reasoned that intracellular localization could impact enzyme availability. Intracellular distribution of GAPDH was assessed due to its recently determined nuclear functions, in addition to its well-established metabolic role to catalyzes the conversion of glyceraldehyde 3-phosphate to glycerate 1, 3-bisphosphate in the cytoplasm (Mazzola and Sirover, 2003). Intriguingly, in naïve CD8+ T-cells GAPDH was predominantly localized in the nucleus (**Figure 13C**, upper panel). By contrast, GAPDH was detected both in the nucleus and the cytoplasm of effector memory CD8+ T-cells (**Figure 13C**, lower panel). Despite the observed similarities in protein expression levels, enhanced cytoplasmic expression of GAPDH may contribute to increased aerobic glycolysis in effector memory CD8+ T-cells immediately after TCR and CD28 ligation.
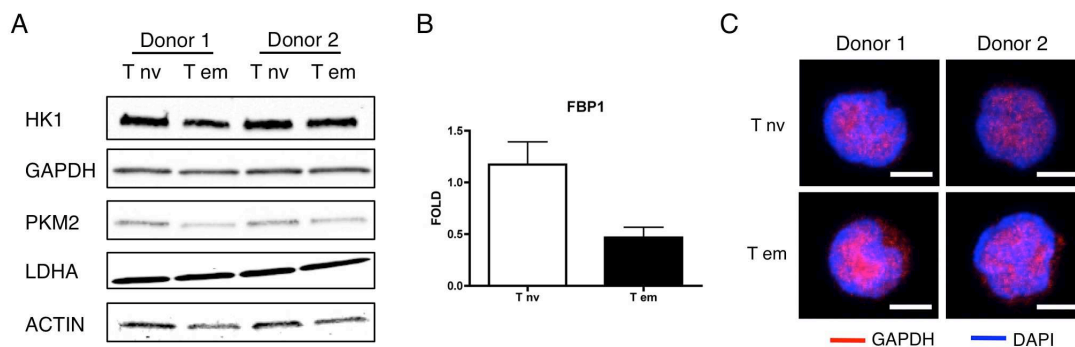

Figure 13. Key enzymes of the glycolytic machinery in naïve and effector memory CD8+ T-cells.

(**A**) Immunoblot analysis of key glyocolytic enzymes, using whole cell lysate of fresh-sorted naïve and effector memory CD8+ T-cells. Actin served as the loading control. Results from 2 of 4 independently assessed donors are shown.

(**B**) Relative FBP1 mRNA expression between naïve and effector memory CD8+ T-cells. Both transcripts were normalized to actin mRNA levels (n=7 donors, ±SD).

(**C**) Stacked confocal microscopy images of naïve and effector memory CD8+ T-cells stained with anti-GAPDH mAb (red), counterstained with DAPI (blue; nucleus). Representative of n=3 independently assessed donors. Magnification = x100, scale bars = 3 µm.

Cytoplasmic GAPDH has been shown to possess higher glycolytic activity than GAPDH compartmentalized in the nucleus (Mazzola and Sirover, 2003). Hence against this background, GAPDH functional capacity was compared between naïve and effector memory CD8+ T-cells. In line with the distribution-pattern, GAPDH functional activity was consistently higher among effector memory CD8+ T-cells (**Figure 14A**). Availability and functional capacity of GAPDH thus plausibly supports the enhanced glycolytic activity observed among effector memory CD8+ T-cells.
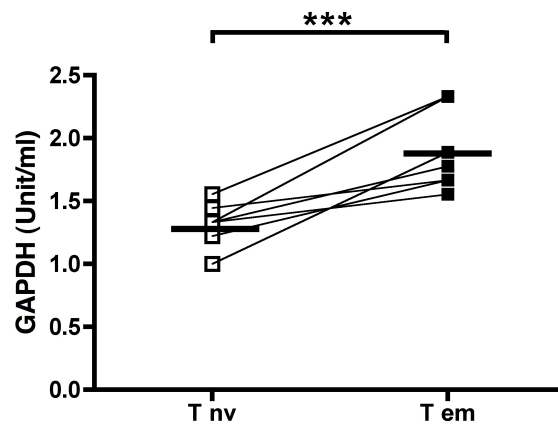

Figure 14. GAPDH activity in naïve and effector memory CD8+ T-cells.

GAPDH activity is higher in freshly sorted effector memory (■) CD8+ T-cells T-cells compared to naïve naïve (□) CD8+ T-cells. *** indicates p=0.0009 (paired student t-test).

Activation induced glycolysis is intrinsic to effector memory CD8+ T-cells

The ability to upregulate aerobic glycolysis is critical for expansion and maturation of effector CD8+ T-cells (Fox et al., 2005). We therefore assessed the glycolytic potential of naïve and effector memory cells under activating conditions, as opposed to chemically induced metabolic stress. To evaluate changes in glycolysis following αCD3 and αCD28 monoclonal antibody (mAb)-stimulation, an *'in-Seahorse'* T-cell activation model was developed. In an initial set of experiments, a low (0.2 µg/mL) or high (10 µg/mL) dose of αCD3 mAb (clone Hit3a), together with a fixed dose of αCD28 mAb (20 µg/mL, clone 28.2), were applied onto plated cells in the metabolic flux analyzer, and real-time changes in ECAR were monitored. Activation of naïve CD8+ T-cells in this setting led to a rapid rise in ECAR, irrespective of the concentration of αCD3 mAb applied (**Figure 15A and 15B**, open symbols). This increase in ECAR, however, was not sustained (**Figure 15A and 15B,** open symbols) and eventually returned to pre-activation levels (**Figure 15C and 15D**). In analogous experiments, activation of effector memory CD8+ T-cells also led to a rapid rise in ECAR (**Figure 15A and 15B,** filled symbols). In contrast to naïve cells, however, ECAR levels of effector memory CD8+ T-cells were maintained at approximately 5 mpH/min, irrespective of the concentration of αCD3 mAb used (**Figure 15A and 15B,** and **15E and 15F**).
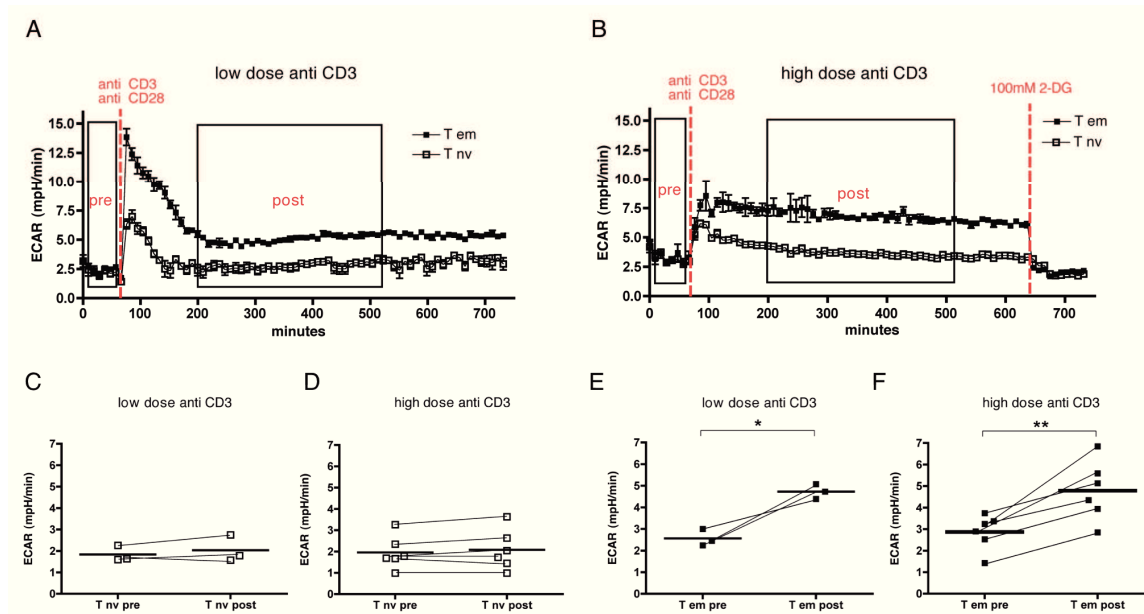
Figure 15. Glycolytic activity of naïve and effector memory CD8+ T-cells upon TCR and CD28 mediated activation.

(**A**, **B**) Representative ECAR graphs of naïve (□) and effector memory (■) CD8+ T-cells treated *'in-Seahorse'* with αCD3 mAb at either low dose (0.2 µg/mL; **A**), or high dose (10 µg/mL; **B**), together with a fixed dose of αCD28 mAb (20 µg/mL). The time-point of antibody injection is marked with a dashed red line. Mean ECAR were measured pre- and post-antibody injection (boxes). Note that injection of 2-deoxy-D-glucose (2-DG) completely and rapidly abolished glycolysis (**B**).

(**C**-**F**) Mean ECAR values of *'in-Seahorse'* CD8+ T-cell activation-experiments. The ECAR of naïve **(C, D)** and effector memory (E, F) CD8+ T-cells were determined pre- and post-injection of low dose (**C**, **E**) and high dose **(D, F)** αCD3 mAb plus αCD28 mAb. Pooled paired data from n=3 (low dose), and n=6 (high dose) independent experiments/donors are shown. * indicates p=0.03, ** p=0.004 (paired Student t-test).

See also **supplementary Figure S7**

To verify that the rise in ECAR was due to increased glucose utilization we added 2-deoxy-D-glucose (2-DG) to activated cells at 600 min post-stimulation **(Figure 16B)**. Injection of 2-DG completely abolished activation-induced glycolysis in both CD8+ T-cell subsets, establishing that the increase in ECAR is due to increased glucose flux along the glycolytic pathway (**Figure 16B**). There was no significant difference in the OCR of both subsets during the post-activation interval probed in these experiments (**Figure S7A and S7B**). Of note, upon injection of 2-DG at 600 min post-stimulation, elevated OCR levels were observed in both subsets (**Figure S7C**).

We further performed additional "*in-Seahorse*" T-cell activation experiments with freshly isolated bulk CD8+ T-cells in absence of glucose **(Figure 17)**. As expected CD8+ T-cells in the glucose free medium had a lower basal ECAR compared to the cells in complete medium and showed unchanged ECAR levels following αCD3 (1 µg/mL) and αCD28 (10 µg/mL) monoclonal antibody (mAb)-stimulation.
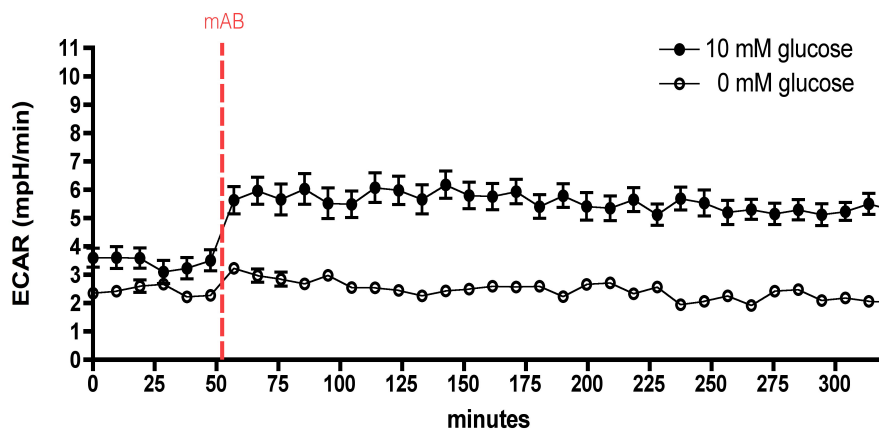

Figure 17. ECAR measurements of bulk CD8+ T-cells in presence and absence of glucose.

Representative ECAR graph of bulk CD8+ T-cells treated *'in-Seahorse'* with αCD3 mAb (1 µg/mL) together with αCD28 mAb (10 µg/mL) in a glucose free medium (O) and glucose (10mM) containing medium (●).

Lastly, as an independent read-out for glycolytic activity, lactate concentrations were measured in the supernatant of non-activated and activated naïve and effector memory CD8+ T-cells. 3 hours after activation, in line with the ECAR data, concentrations of lactate were higher in the supernatant of both αCD3/CD28 mAb activated T-cell subsets. As an internal control, effector memory CD8+ T-cells being activated in a glucose free medium did not produce any lactate **(Figure 18A)**. In addition, this increase was more pronounced in the effector memory subset compared to naïve CD8+ T-cells **(Figure 18B)**.
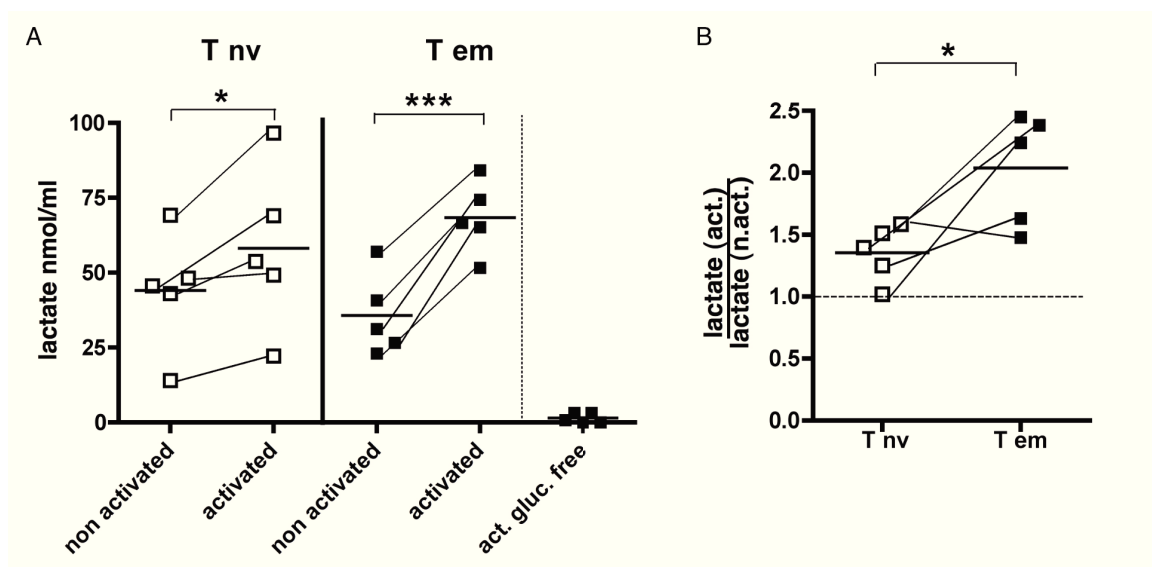

Figure 18. Lactate concentrations in the supernatant of naïve and effector memory CD8+ T-cells upon TCR and CD28 mediated activation.

(A) Activation with the high dose (10 µg/mL) αCD3 mAb in combination with αCD28 mAb (20 µg/mL,) leads to significant increase of lactate levels in the supernatant after 3 hours. No lactate was detectable in the supernatant of activated effector memory (■) T cells being in a glucose free medium. Pooled paired data and mean values from 5 independent experiments/donors are shown. * indicates p=0.045, *** p=0.0007 (paired Student t-test).

(B) The ratio of lactate levels "activated" to "non activated" for paired subsets was used to compare the increase of lactate production between both populations. Data and mean values from n=5 donors are shown. A generalized linear model was used to calculate an interaction p-value between the two variables. * indicates p=0.003 (linear regression model)

To exclude the possibility that non-specific binding of αCD3 mAb was responsible for the observed increase in ECAR, control experiments were performed using an appropriate isotype control mAb in combination with αCD28 mAb. There was no detectable increase in ECAR for both subpopulations following exposure of cells to isotype control antibody (**Figure 19A**). Sustained activation-induced levels in ECAR among effector memory, but not naïve CD8+ T-cells indicated that aerobic glycolysis is differentially regulated between both subsets. We next probed the individual contribution of TCR/CD3 stimulation vs. co-stimulatory (CD28) signaling in mediating this differential effect. There was no observable increase in ECAR when cells were treated with low dose (0.2 µg/mL) αCD3 mAb, whereas high dose (10 µg/mL) αCD3 mAb induced a transient increase (**Figure 19B**). Moreover, stimulation with αCD28 mAb alone (20 µg/mL) did not have any effect on ECAR (**Figure 19C**). As demonstrated above, the sustained increase in ECAR was again only observed among effector memory CD8+ T-cells treated with both αCD3 and αCD28 mAb (**Figure 19D**). These results indicate that, although CD3 clustering is sufficient to briefly activate aerobic glycolysis in effector memory CD8+ T-cells, CD28 signaling is critical for a *sustained switch* to aerobic glycolysis.
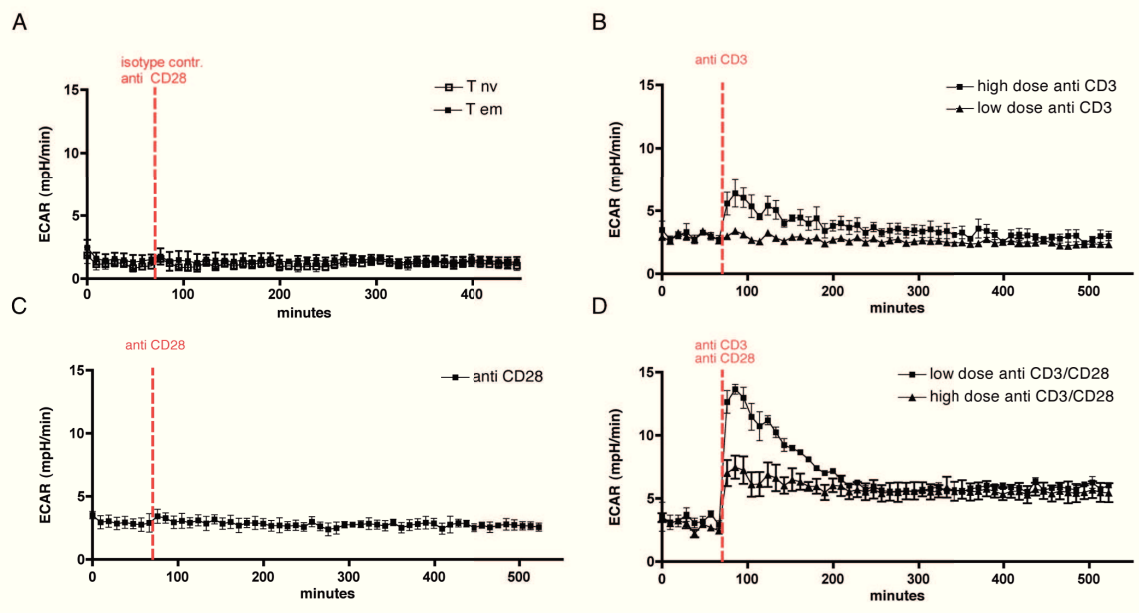
Figure 19. Sustained glycolytic switch in effector memory CD8+ T-cells needs a combined activation of TCR and CD28.

(A) ECAR graph of naïve and effector memory CD8+ T-cells treated *'in-Seahorse'* with isotype control mAb (mIgG2a, control for αCD3 mAb (10 µg/mL)), plus αCD28 mAb (20 µg/mL).

(B-D) ECAR graphs of effector memory CD8+ T-cells treated *'in-Seahorse'* with low (0.2 µg/mL), and high dose (10 µg/mL) αCD3 mAb alone (**B**), αCD28mAb (20 µg/mL) alone (**C**), or αCD3 mAb combined with αCD28 mAb (**D**).

Next, we tested whether naïve and effector memory CD8+ T-cells differ in their ability to increase glucose uptake. To probe for this, we measured the uptake of NBDG –a fluorescent glucose analog– by both subsets following stimulation with αCD3 and αCD28 mAb. In total naïve CD8+ T-cells, antibody treatment did not induce an increase in NBDG uptake (**Figure 20A**, left panel). In contrast, NBDG uptake was consistently, although moderately, increased in total effector memory CD8+ T-cells following stimulation (**Figure 20A**, right panel). When gating on blasting CD8+ T-cell subsets (characterized by increased forward scatter [FSC]– **Figure 20B**), the differential capacity for glucose uptake became even more apparent (**Figure 20C**). Thus, in addition to potential FBP1-related differences in glucose flux and differences in the cytoplasmic availability of GAPDH, a differential capacity to support glycolysis from external glucose sources is present between naïve and effector memory CD8+ T-cells.
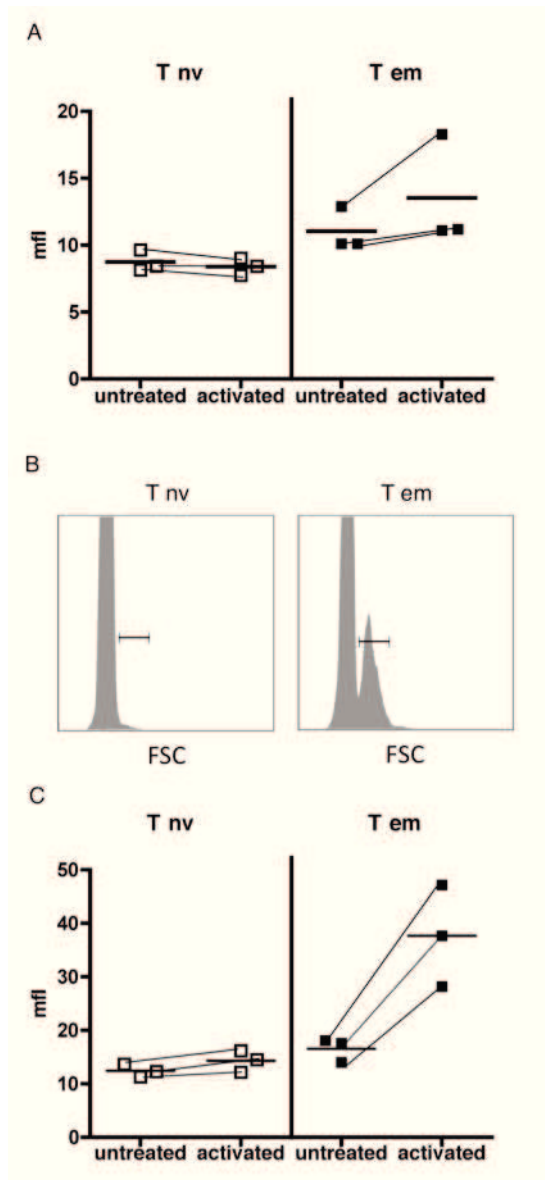
Figure 20. Glucose uptake by naïve and effector memory CD8+ T-cells upon TCR and CD28 mediated activation.

(**A**) Uptake of NBDG, a fluorescent glucose analog, by bulk naïve and effector memory CD8+ T-cells that were either left untreated, or activated for 45 minutes with 10 µg/mL αCD3 mAb and 20 µg/mL αCD28 mAb.

(**B,C**) Uptake of NBDG as described in (**A**), gating on 'blasting' naïve and effector memory CD8+ T-cells. (**B**) Inserts show representative forward scatter (FSC) histograms of naïve and effector memory CD8+ T-cells, with the population gated for assessing NBDG uptake indicated (**C**). Data and mean values of 3 independent experiments/donors are shown. * indicates p=0.04 (paired Student t-test).

46

Contribution of the PI3K/AKT/mTOR axis to immediate-early glycolytic switch in effecroe memory CD8+ T-cells

CD28 co-stimulation during T-cell activation enhances glucose utilization via signaling along the PI3K/AKT/mTORC1 pathway, which leads to increased cell growth and proliferation (Frauwirth et al., 2002a). The signaling events downstream of CD28 critical for early increase in glycolysis intrinsic to effector memory CD8+ T-cells are not known. To address this issue, *'in-Seahorse'* αCD3/αCD28 activation experiments were carried out using effector memory CD8+ T-cells pre-treated with LY294002 (10 µM, PI3K inhibitor), AKTi 1/2 (10 µM, AKT inhibitor), and rapamycin (20 ng/mL, mTORC1 inhibitor) (**Figure 21**). Inhibition of PI3K (**Figure 22A**) and AKT (**Figure22B**) completely abolished activation induced, immediate-early glycolytic phase in effector memory CD8+ T-cells. Intriguingly, immediate-early glycolytic phase was refractory to rapamycin treatment (**Figure 22C**).
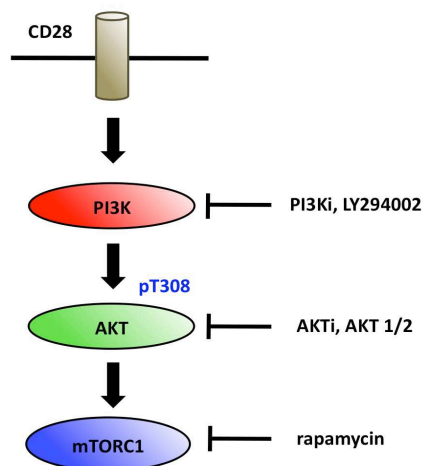

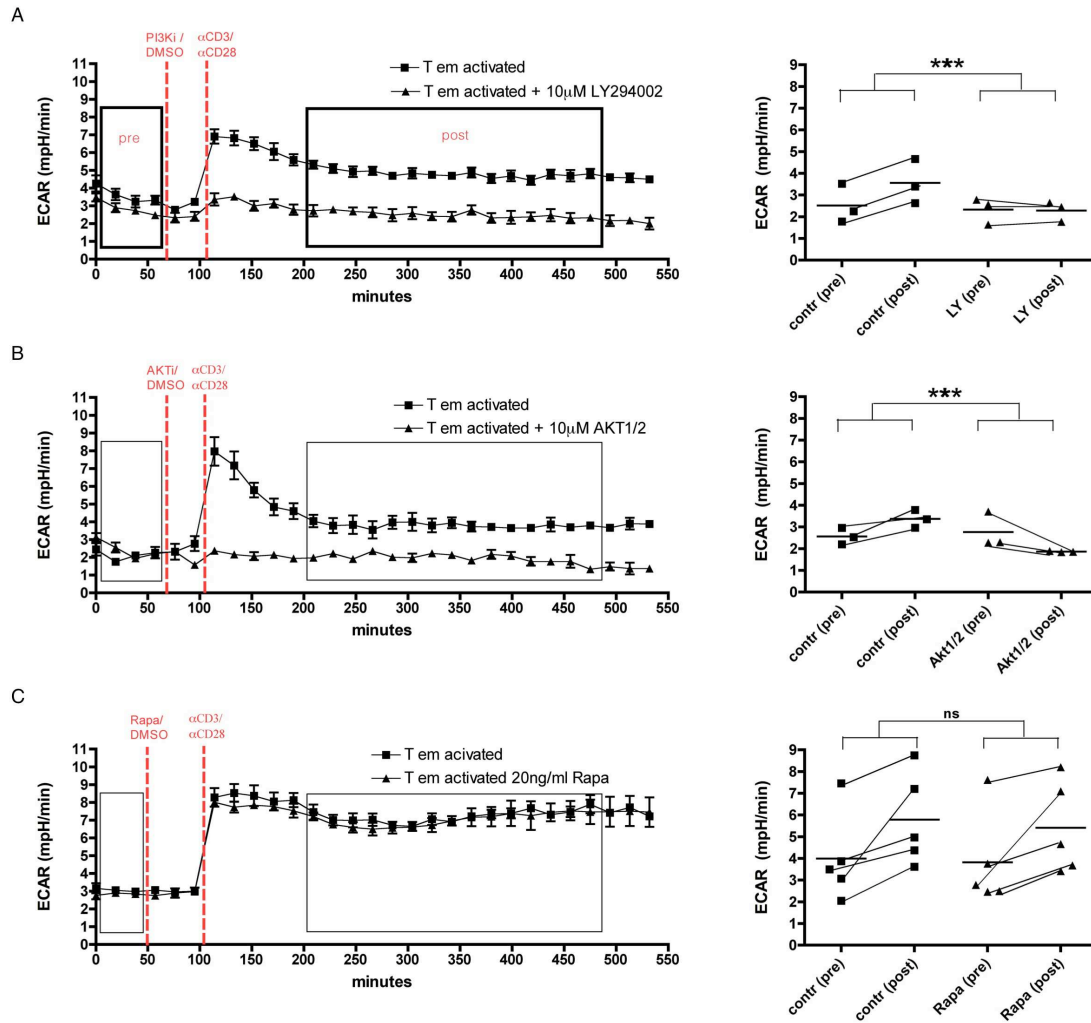**Figure 21. Model of CD28 signaling along the PI3K/AKT/mTORC1 pathway**

Figure 22. Glucose uptake by naïve and effector memory CD8+ T-cells upon TCR and CD28 mediated activation.

(**A-C, left side**) Representative ECAR graphs of naïve and effector memory CD8+ T-cells treated *'in-Seahorse'* with αCD3 mAb at (1 μg/mL) together with αCD28 mAb (10 μg/mL). PI3K, AKT and mTORC1 inhibitors (▲) or DMSO control (■) have been injected to the wells 30-50 min prior to activation. Time-points for injection of the inhibitors and activation antibodies are marked with a dashed red line. Mean ECAR were measured pre- and post-antibody injection (boxes). To calculate the impact of each inhibitor a linear regression model was used to compare the paired groups (**A-C, right side**).

(**A and B**) Pretreatment of CD8+ memory T-cells with 10mcM Ly294002 (**A**) or 10mcM AKTi 1/2 (**B**) inhibited early-immediate glycolytic switch significantly (n=3 each). *** indicate p<0.0001 (linear regression model)

(**C**) Injection of 20ng/ml rapamycin did not affect increase in ECAR after activation (n=5).

mTORC1 is a known regulator of glycolysis in proliferating T-cells (Finlay et al., 2012; Fox et al., 2005). Thus, we investigated the effect of rapamycin on the glycolytic capacity of both CD8+ T-cell subpopulations after long-term activation (**Figure 23A and B**). Compared to non-stimulated cells, ECAR was enhanced in both naïve (**Figure 23A**) and effector memory (**Figure 23B**) CD8+ T-cells stimulated for 3 days with αCD3/αCD28 mAbs. However, when activated in the presence of rapamycin (20 ng/mL), there was a marked reduction in ECAR between both subsets suggesting that the protracted phase of aerobic glycolysis is sensitive to mTORC1 inhibition (**Figure 23A and B**).
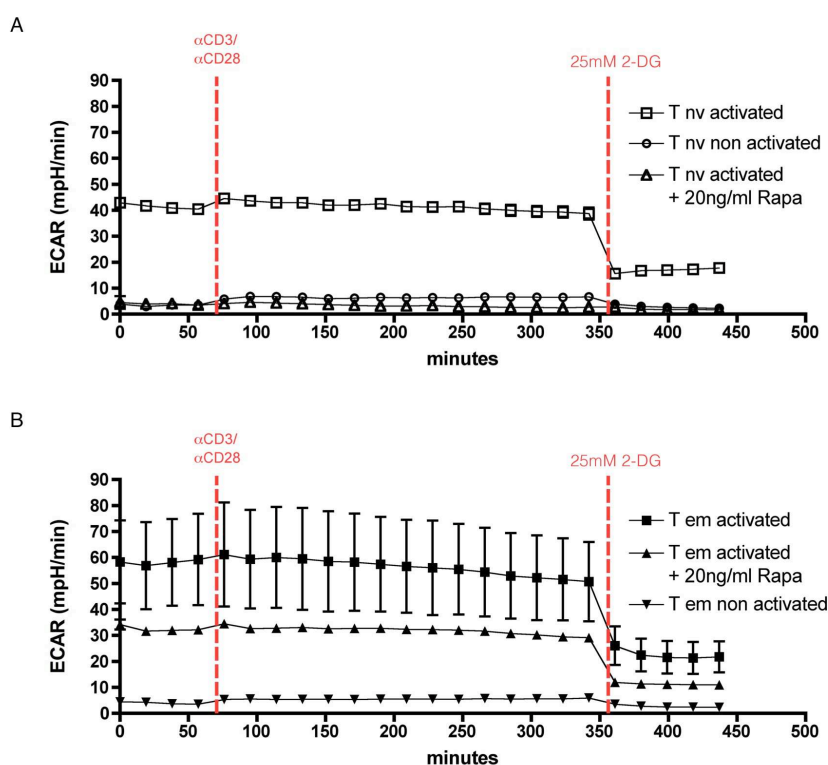

Figure 23. Rapamycin inhibits protacted phase of aerobic glycolyis in naïve and memory CD8+ T-cells.

Sorted naïve (**A**) and effector memory (**B**) CD8+ T-cells have been activated for 3 days with αCD3 (1 µg/mL) and αCD28 (10 µg/mL) in the presence or absence of 20ng/ml rapamycin. Rapamycin decreased the protacted phase of aerobic glycolyis in both subsets. Additional re-stimulation in the seahorse with the same dose had a minimal effect on ECAR in both subsets (first dashed red line). Note that injection of 2-deoxy-D-glucose (2-DG) rapidly decreased ECAR.

Effect of CD28 pathway inhibitors on proliferation

Aerobic glycolysis is essential for providing energy and metabolic intermediates in highly proliferating cells (Vander Heiden et al., 2009). In the presence of PI3K-, AKT- and mTORC1-inhibitors, proliferation of effector memory CD8+ T-cells was blocked (**Figure 24**). These results indicate that the PI3K→AKT→mTORC1 pathway is essential for effector memory T-cell expansion, potentially via the regulation of aerobic glycolysis in highly proliferating CD8+ T-cells. More importantly, using the metabolic flux analyzer, we discriminated two distinct glycolytic phases in effector memory CD8+ T-cells: the rapamycin-insensitive immediate-early phase, and the rapamycin-sensitive protracted phase which is essential to support CD8+ T-cell proliferation.
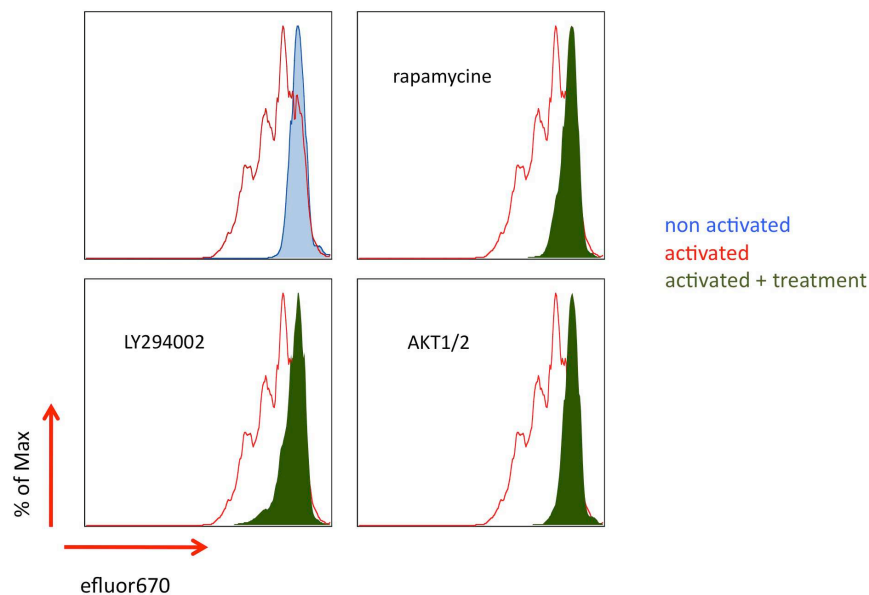

Figure 24. Proliferation of effector memory CD8+ T-cells is affected by various CD28 pathway inhibitors.

Effector memory CD8+ T-cells were loaded with eFLuor-APC. Compared to non activated control cells (blue shaded) activation (red line) with αCD3 (2µg/mL) and αCD28 (20µg/mL) led to a robust proliferation assessed after 3 days in culture (top left). Activation in the presence of all three inhibitor (green shaded) efficiently blocked proliferation. Representative histograms of 3 independent experiments are shown.

Phosphorylation on Ser473 is critical for immediate-early glycolytic switch

Abrogation of glycolysis in effector memory CD8+ T-cells pre-treated with LY294002 and AKTi 1/2 indicates that AKT plays a central role in regulating immediate-early glycolytic switch. AKT activity is dependent on the phosphorylation of two residues: Thr308 and Ser473. AKT-Thr308 is a target of PDK1, and AKT-Ser473 is phosphorylated by mTORC2, which allows AKT to act on additional substrates involved in cell metabolism and survival (Guertin et al., 2006). Recently, mTORC2 activity has been shown to be directly activated by the PI3K product PtdIns(3,4,5)P3 (Gan et al., 2011). Thus PI3K could also impact AKT activity indirectly by modulating mTORC2 activity. To investigate a possible role of mTORC2 in immediate early glycolytic switch, effector memory CD8+ T-cells were pre-treated with OSI-027 (1 µM), an mTORC1/C2 inhibitor, and changes in ECAR levels following αCD3/αCD28 mAb activation were assayed as above. Interestingly, inhibition of mTORC1/C2 resulted in a non-sustainable increase in ECAR that eventually returned to baseline levels (**Figure 25A and B**). Analogous to rapamycin, OSI-027 treatment also blocked cell proliferation (**Figure 25C**). To probe for an effect of OSI-027 on mTORC2 activity, we compared AKT-S473 and AKT-T308 phosphorylation in activated effector memory CD8+ T-cells by immunoblot analyses (**Figure 25D**). AKT-T308 and AKT-S473 phosphorylation was increased in activated effector memory CD8+ T-cells. Activation of effector memory cells in the presence of either rapamycin or OSI-027 maintained pT308 levels. However, OSI-027 dramatically reduced pS473 in activated effector memory cells, whereas, pS473 was insensitive to rapamycin. Under identical conditions we also probed for phosphorylation of 4EBP1 (Thr37/46), a downstream target of mTORC1 (Laplante and Sabatini, 2012), (**Figure 25D**). 4EBP1 phosphorylation was increased in activated effector memory CD8+ T-cells. Inhibition of mTORC1 activity either with rapamycin or OSI-027 lead to reduction of p4EBP1 levels. The sensitivity of immediate early glycolytic switch to mTORC2 inhibition indicates that AKT phosphorylation at Ser-473 is critical for this event (**Figure 25D and Figure S8).**
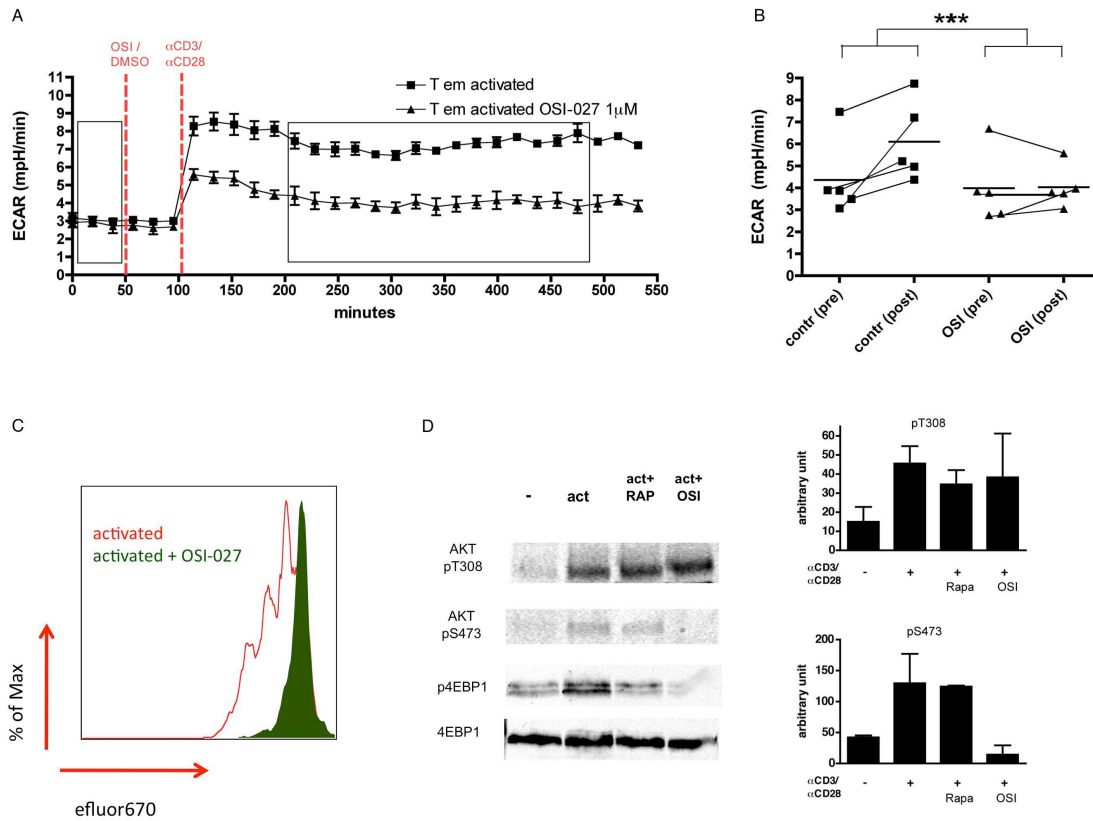
Figure 25. Immediate-early glycolytic switch in effector memory CD8+ T-cells is dependent on mTORC2 and AKT activity.

(**A and B**) Representative ECAR graph (**A**) and pre-/post-activation mean ECAR (n=5) (**B**) of effector memory CD8+ T-cells pre-treated with control-media/DMSO (■) or 1 μM OSI-027 (▲) prior to activation. *** p<0.001 (linear regression model)

(**C**) Representative histogram of OSI-027 treated EM CD8+ T-cells, similar strategy as described in **Figure 24**.

(**D**) Immunoblot and quantitative analyses (in arbitrary units) of effector memory CD8+ T-cells, 3 hours post αCD3/αCD28 mAb (2 μg/mL and 20 μg/mL) activation with or without rapamycin (20 ng/mL) or OSI-027 (1 μM). Blots were probed for AKT pT308 and pS473, total 4EBP1, and phospho-4EBP1.

See also s**upplementary Figure S8**

IFN-γ synthesis by effector memory CD8+ T-cells is dependent on glucose

Effector memory CD8+ T-cells contain preformed cytotoxic granules and are able to rapidly upregulate cytokines such as IFN-γ and TNF-α. Interestingly, IFN-γ synthesis of effector CD8+ T-cells is intimately linked to glucose metabolism (Cham et al., 2008; Cham and Gajewski, 2005a). Given the rapid upregulation of glycolytic flux in αCD3/αCD28 mAb stimulated effector memory CD8+ T-cells, we assessed the role of the immediate-early glycolytic phase on CD8+ T-cell activation and elaboration of effector molecules. Specifically, we probed for expression of the activation marker CD69, and assessed IFN-γ production in quiescent and activated naïve and effector memory CD8+ T-cells. In naïve T-cells, the frequency of CD69 expressing T-cells increased significantly following activation (**Figure 26A and B**). By contrast, IFN-γ remained undetectable after 12 hours of stimulation (**Figure 26C**) indicating that IFN-γ synthesis in previously unprimed human CD8+ T-cells requires prolonged activation.
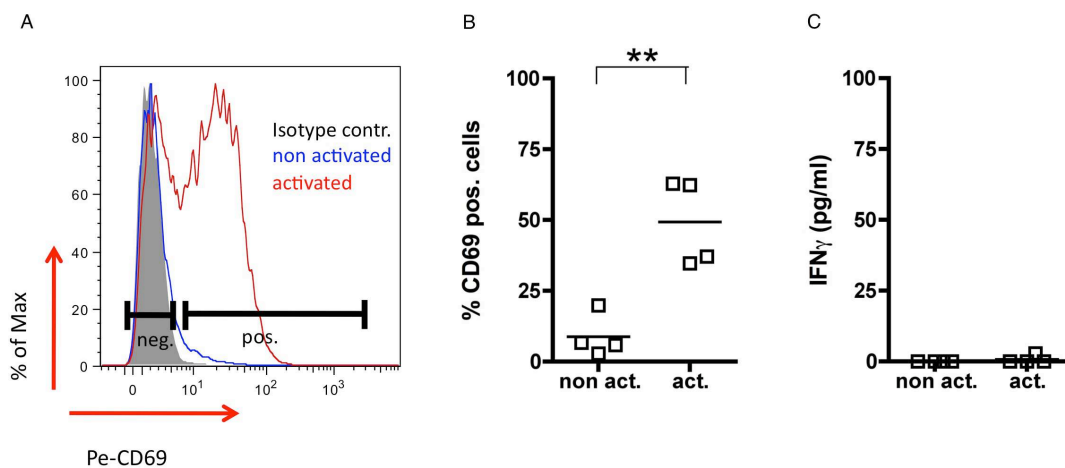

Figure 26. CD69 expression and IFN-γ production of naïve CD8+ T-cells

(**A and B**) Cell-surface expression of CD69 on naïve CD8+ T-cells was compared between αCD3/αCD28 mAb (2 µg/mL and 20 µg/mL) activated and non-activated cells (8h incubation) (n=4). A representative histogram (**A**) depicts CD69 expression on naïve cells cultured under non-activating (blue line) and activating (red line) conditions. Using an isotype control antibody (black shaded) cells were defined as CD69 negative or positive. Activation led to a higher percentage of CD69 positive cells compared to non activated naïve CD8+ T-cells (**B**). ** indicates p=0.007 (paired Student t-test).

(**C**) IFN-γ production by naïve CD8+ T-cells was compared between non-activated and αCD3/αCD28 mAb (2 µg/mL and 20 µg/mL) activated cells (12h incubation) (n=4)

Effector memory CD8+ T-cells also upregulated CD69 following activation (**Figure 27A and B**). In contrast to naïve cells, however, IFN-γ production by effector memory CD8+ T-cells was elevated at 12 hours post-stimulation (**Figure 27C**). To determine the role of the AKT→mTORC1 axis in early effector memory CD8+ T-cell activation, cells were treated with AKTi 1/2 or rapamycin (as above). CD69 surface expression remained elevated under both treatment conditions, albeit the frequency of CD69+ cells was slightly decreased in AKTi 1/2 treated cells (**Figure 27B**). Interestingly, AKT inhibition resulted in a clear reduction of IFN-γ production by effector memory CD8+ T-cells, whereas rapamycin treatment had no impact on early IFN-γ synthesis (**Figure 27C**). The dependence of early IFN-γ production on AKT suggested that immediate-early glycolytic switch likely plays a role in this effector response.
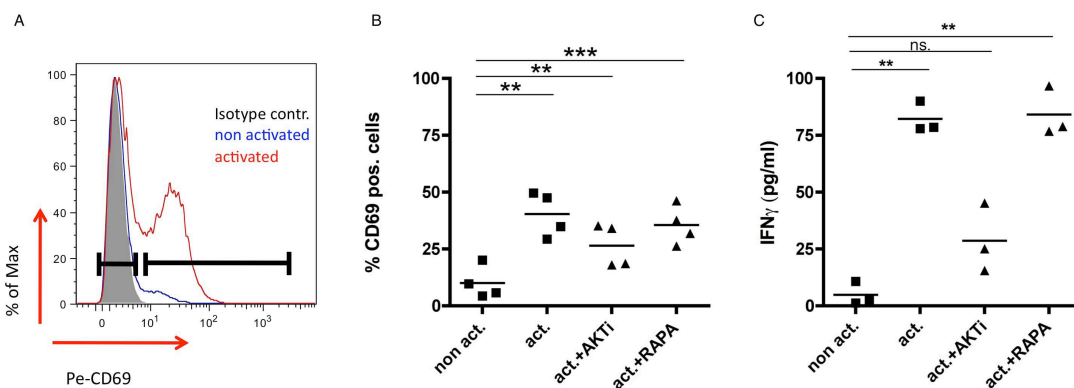
Figure 27. CD69 expression and IFN-γ production of effector memory CD8+ T-cells

(**A and B**) Representative histogram (**A**) shows CD69 expression on effector memory CD8+ T-cells cultured under conditions as mentioned in (**Figure 26**). To determine the role of the AKT/mTORC1 axis in early activation, effector memory CD8+ T-cells were additionally treated (**B**) with AKTi 1/2 (10 □M) and rapamycin (20ng/mL).

(**C**) IFN-γ production by effector memory CD8+ T-cells was compared between non-activated and αCD3/αCD28 mAb activated cells; ± AKTi 1/2 (10 □M); ± rapamycin (20ng/mL) (12h incubation) (n=3).

To directly probe for the dependence of effector memory T-cell CD69 expression and IFN-γ production on glucose availability, cells were activated in the presence of different gluose concentrations. In all the experiments that were assessing proliferation, CD69 upregulation or IFN-γ production, 10% human serum was always added 3 hours after activation. However, human AB serum contains around 5mM glucose. Blocking glycolyis by adding 2-deoxyglucose (2-DG) circumvent this issue. Glucose free medium with additon of serum was named "low glucose", containing around 0.5 mM (**Figure 28**).

ID	glucose 10mM	Inhibitor	mAB 2/20	serum 10%
non act.	yes	no	no	yes
act. (Figure 20C)	yes	no	yes	yes
low gluc	no	no	yes	yes
low gluc+2DG	no	2DG 10mM	yes	yes
no gluc / no serum	no	no	yes	no

Figure 28. Detailed information about glucose availability conditions used in Figure 29

The frequency of CD69 positive cells was similar for all three conditions, establishing that early effector memory T-cell activation can occur independently of glucose availability (**Figure 29A**). IFN-γ production remained elevated in the presence of 0.5 mM glucose (**Figure 29B**). However, upon addition of 2-DG and under glucose-free conditions, IFN-γ production was greatly diminished (**Figure 29B**). These findings indicate that IFN-γ recall response in effector memory CD8+ T-cells is highly dependent on immediate-early glycolytic capacity. Moreover, these experiments correlate AKT activity to effector memory CD8+ T-cell IFN-γ production via mediating an immediate-early glycolytic switch and thus increased glucose metabolism.
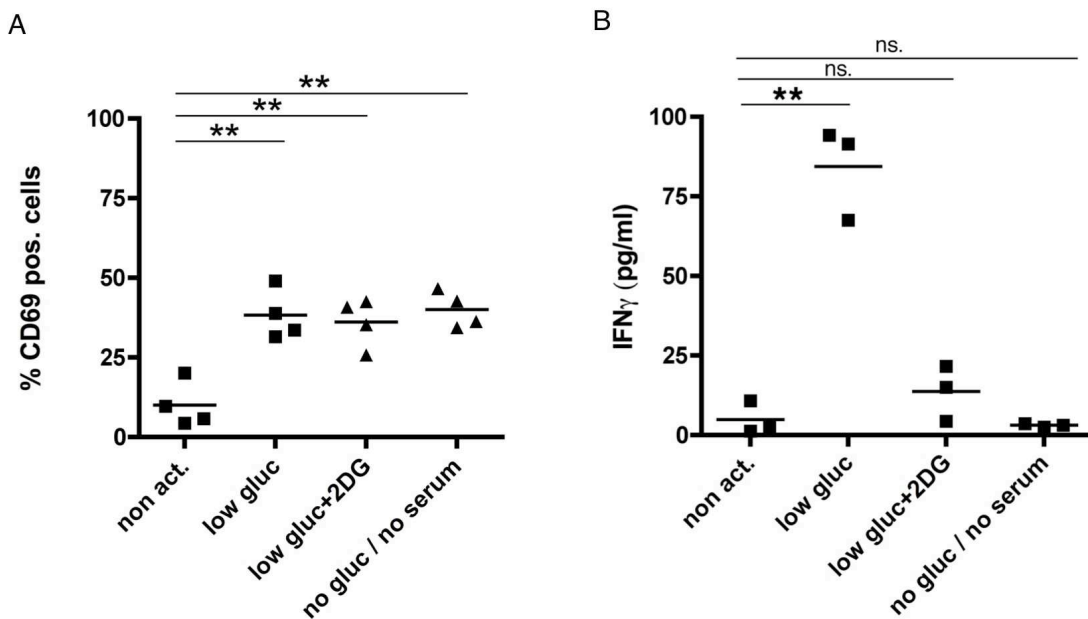
Figure 29. CD69 upregulation and IFN-γ production of effector memory CD8+ T-cells

(**A**) Cell-surface expression of CD69 on effector memory CD8+ T-cells was compared between non-activated and αCD3/αCD28 mAb activated cells in presence of low glucose (0.5 mM); glucose + 2DG; or no glucose / no serum (8h incubation) (n=4).

(**B**) IFN-γ production by effector memory CD8+ T-cells was compared between non-activated and αCD3/αCD28 mAb activated cells in presence of low glucose (0.5 mM); low glucose + 2DG; or no glucose/no serum (12h incubation) (n=3).

DISCUSSION

Important qualitative differences exist between naïve and memory CD8+ T-cells in their response to cognate antigen (Cui and Kaech, 2010). During secondary infections, memory CD8+ T-cells are able to respond and acquire effector function more rapidly than naïve cells. Numerous reports have described functional and cell surface phenotypic differences between naïve and memory CD8+ T-cells. Relatively few studies, however, have investigated the metabolic repertoire –and its impact on cellular functionality– of these key CD8+ T-cell populations. Experiments detailed in this report show that human naïve and effector memory CD8+ T-cells possess distinct metabolic signatures. This was demonstrated by differences in mitochondrial respiratory capacities, mitochondrial mass and morphology, cellular substrate utilization and glycolytic potential.

Using the Seahorse extracellular flux analyzer, we characterized the metabolic repertoire of human naïve and effector memory CD8+ T-cells. Drugs affecting mitochondrial respiration were used to define differences in glucose and fatty acid metabolism in both CD8+ T-cell subsets. Later, 'in-Seahorse' TCR and CD28 stimulation assays were performed to assess, in real-time, the role of these distinct signaling pathways in the remodeling of CD8+ T-cell metabolic repertoire. Several control experiments, such as activation in glucose-free medium, addition of glycolysis inhibitors or lactate measurements using an independent technique, demonstrated the reliability of the Seahorse system to assess metabolic signatures.

In the first section of the discussion, the focus will be set on steady state differences between two CD8+ T-cell subsets. The impact of metabolic repertoires on activation-induced changes will be discussed in the second section. Critical points will be addressed in the final section.

I. Metabolic repertoire of naïve and effector memory CD8+ T-cells

The SRC of effector memory CD8+ T-cells was significantly higher than in their naïve counterparts. This respiratory parameter has been implicated in the ability of cells to rapidly respond to higher energy demands, and in the control of reactive oxygen species. In mice, memory CD8+ T-cells have recently been shown to also have higher SRC than their naïve counterparts, and the SRC was mechanistically linked to memory differentiation (van der Windt et al., 2012). The parallel finding of increased SRC in both human and murine memory CD8+ T-cells indicates that this trait likely reflects an important feature of memory CD8+ T-cell functionality.

Congruent with higher SRC in effector memory CD8+ T-cells, an increase in mitochondrial mass was also observed in this subpopulation. Moreover, a consistent feature of effector memory CD8+ T-cells was the presence of distinct MTG^{bright} and MTG^{dim} populations. Given this observation, it is interesting to note that the mitochondrial mass of HIV- and CMV-specific effector memory CD8+ T-cells, from the same donor, were found to have a similar mass distribution –with HIV-specific cells possessing higher mitochondrial mass than their CMV-specific counterparts (Petrovas et al., 2007). This suggests that metabolic heterogeneity exists amongst effector memory CD8+ T-cells. It will be interesting to assess whether metabolic heterogeneity associates with functional differences in effector memory T-cells, as defined by phenotypic markers such as CD27 and CD28 (Romero et al., 2007). In addition, effector memory CD8+ T-cells displayed greater mitochondrial length and complexity than naïve cells. Dynamin related protein 1 (DRP1), a mediator of mitochondrial fission, is an established and important regulator of T-cell activation (Baixauli et al., 2011). It can be postulated that tubular mitochondria in effector memory CD8+ T-cells allow for mitochondrial fission to occur more readily, without the prerequisite mitochondrial biogenesis-step typically observed following naïve T-cell activation (D'Souza et al., 2007). Whether mitochondrial mass and morphology impact the recall response of effector memory CD8+ T-cells remains to be elucidated.

It was previously demonstrated that fatty acid oxidation (FAO) is enhanced in mouse CD8+ T-cells during effector to memory differentiation (Pearce et al., 2009). We were able to extend these findings by showing that the same pattern persists in human CD8+ T-cells. Effector memory CD8+ T-cells increased oxygen consumption more than naïve CD8+ T-cells in the presence of palmitate. In line with this functional difference, FATP2, an important transporter for free fatty acids (Falcon et al., 2010), was elevated on both mRNA and protein level in effector memory T-cells.

A further defining metabolic feature of memory CD8+ T-cells was their selective, digital signaling-like capacity to upregulate aerobic glycolysis. Protein expression levels of key glycolytic enzymes (HK1, GAPDH, PKM1/2, PKM2, and LDHA) were similar in naïve and effector memory subsets. However, enzymatic activity is subject to regulation at various levels (e.g. post-translational modifications, oligomerization state of enzymes, allosteric regulation, and cellular localization). Whether the difference in glycolytic capacity observed here is due to differential enzymatic regulation remains to be investigated. Cellular distribution of GAPDH protein expression was clearly distinct between naïve and effector memory CD8+ T-cells. GAPDH in naïve cells was primarily localized in the nucleus. In contrast, GAPDH expression in effector memory cells was equally detected in both nuclear and cytoplasmic compartments. Cytoplasmic GAPDH has been shown to possess higher glycolytic activity than GAPDH compartmentalized in the nucleus (Mazzola and Sirover, 2003). In line with this we show a higher GAPDH activity in effector memory CD8+ T-cells, likely contributing to the higher glycolytic capacity observed. Nucleus-localized GAPDH, on the other hand, has been shown to mediate the trans-nitrosylation and inhibition of Sirtuin 1 (SIRT1), an essential regulator of energy metabolism (Kornberg et al., 2010). Hence, nucleus-localized GAPDH of CD8+ T-cells likely has additional, as yet unidentified effects on CD8+ T-cell metabolic regulation.

Gluconeogenic enzymes antagonize strongly exergonic reactions that promote glucose flux along the glycolytic pathway. Among them, FBP1 catalyzes the hydrolysis of

fructose-1,6-bisphosphate into fructose-6-phosphate. Hypermethylation of FBP1 promoter, resulting in decreased enzyme expression, has been demonstrated to enhance aerobic glycolysis in highly proliferating tumor cells (Liu et al., 2010). Opposing levels of FBP1 mRNA in naïve vs. effector memory CD8+ T-cells suggests that differences in the activity of glycolysis vs. gluconeogenesis pathways may dictate net glucose flux in CD8+ T-cell subpopulations. Such a mechanism for controlling glucose metabolism would likely result in high adaptability to changes in nutrient availability and/or stimulatory conditions.

In all, the steady state metabolic signature of CD8+ T-cell subsets suggests a greater adaptability of effector memory cells to different energy sources compared to naïve cells. Increased SRC and FAO, and the ability of effector memory CD8+ T-cells to rapidly upregulate aerobic glycolysis indicates that these metabolic parameters likely play a significant role in the survival and function of these cells.

II. Activation induced glycolysis in effector memory CD8+ T-cells

T-cell activation is primarily dependent on two signals. Ligation of the TCR/CD3 complex triggers activation of mitogen activated protein kinase (MAPK) signaling pathways, increased intracellular levels of diacylglycerol (DAG) and Ca2+, and activation of the transcription factors NFAT and NF-κB (Smith-Garvin et al., 2009). Co-stimulation through CD28 via its ligands CD80 or CD86, on the other hand, leads to activation of the PI3K–AKT pathway and upregulation of Glut1 expression (Frauwirth et al., 2002a; Jacobs et al., 2008). Aerobic glycolysis was stably increased in effector memory CD8+ T-cells following stimulation with both αCD3 *and* αCD28 antibodies, but not in the absence of CD28 ligation. Interestingly, the absence of CD28 co-stimulation leads to deficits in memory CD8+ T-cells re-expansion due to an inhibition of cell cycle progression (Borowski et al., 2007). Moreover, mice lacking CD80 and CD86 have previously been demonstrated to be important for CD8+ T-cell recall responses (Grujic et al., 2010). Thus, enhanced glycolytic switch in EM cells could play a role in CD8+ T-cell recall response.

The role of CD28 in mediating glucose uptake by increasing GLUT1 expression is well established (Jacobs et al., 2008). We also observed enhanced uptake of 2-NBDG, a glucose analog, by activated memory cells compared to naïve CD8+ T-cells. Our data indicate that memory CD8+ T-cells rely on CD28 signaling *to sustain immediate-early metabolic switch* to aerobic glycolysis. Intriguingly, this switch was insensitive to rapamycin treatment. On the other hand fully phosphorylated AKT on both sites, Thr308 and Ser473, was required. AKT-Thr308 is a target of PI3K via PDK1 and AKT-Ser473 is phosphorylated by mTORC2. Pretreatment with either PI3K inhibitor LY294002, mTORC2 inhibitor OSI-027 or a direct AKT inhibitor AKTi 1/2 blocked the early upregulation of glycolyis efficiently, indicating an important role for AKT in mediating this effect. Although it is well established that LY294002 has an off-target inhibitory effect on mTORC1 (Brunn et al., 1996), this off-target effect can be ruled out as a confounder in these experiments, since rapamycin had

no effect on immediate-early glycolytic phase. Additionally, all the inhibitors efficiently blocked proliferation.

However, It should be noted that such a central role for AKT in T-cell metabolism and proliferation has been questioned recently (Macintyre et al., 2011). Due to different experimental settings comparisons with our or other studies are difficult. For proliferation assays, Macintyre and colleagues activated naïve mouse cells in the presence of αCD3 and IL2. Only at day 5 the inhibitors AKT 1/2 or PI3K inhibitor IC87114 were added for the remaining 2 days. However, it has been shown that early administration of PI3K inhibitors after activation is required to block proliferation efficiently (Soond et al., 2010). As a second readout, Macintyre and colleagues measured uptake of radioactively labeled glucose. Transgenic naïve CD8+ T-cells were activated with the specific gp33 peptide, washed and cultured with 20ng/ml IL2 in the presence of AKTi 1/2 (1 mcM). Addition of AKTi 1/2 did not affect glucose uptake in their experiments. In our experiments, we pretreated human memory CD8+ T-cells witch 10 mcM AKTi 1/2. Therefore several reasons could account for the different findings such as the pretreatment dose of AKT 1/2 or IL2 or the absence of co-stimulatory signals in their assays. In addition, primary expansion and acquisition of immune function are distinct from a secondary immune response. Most mouse studies, including Macintyre et al was performed in vitro using unprimed mouse T-cells. Much less is known regarding the metabolic requirements of secondary immune responses. Thus, further studies will have to be done to evaluate the importance of AKT for T-cell metabolism.

Increased glycolysis after T-cell activation is thought to be important to build intermediates that can produce biomass for proliferation (Vander Heiden et al., 2009). As a central regulator of transcription and protein synthesis mTORC1 plays an important role in this context (Laplante and Sabatini, 2012). Our data confirmed the crucial role of mTORC1 in proliferation. Rapamycin efficiently blocked the proliferation and glycolytic rates of activated naïve and effector memory CD8+ T-cells at day 3 after activation. Thus, the

insensitivity of *immediate-early glycolytic switch* to rapamycin treatment points to a distinct biologic function for the early upregulation of glycolysis in effector memory CD8+ T-cells.

Protective immunologic memory depends on antigen-experienced T-cells that are able to: (a) rapidly acquire effector function and (b) expand as secondary effector cells (Masopust and Picker, 2012). The immediate acquisition of effector function is mediated by effector memory T-cells. Clonal re-expansion, on the other hand, has been assigned to central memory T-cells. Effector memory CD8+ T-cells are heterogeneous ranging from tissue resident, migratory, to blood borne populations (Masopust and Picker, 2012). Tissue resident effector memory (T rm) cells are not accessible with conventional isolation methods since they are not recirculating in the blood (Bevan, 2011). Several models of skin infection in mice showed the importance of these site based memory cells (Gebhardt et al., 2009; Jiang et al., 2012). Circulating effector memory T-cells in the blood contain blood borne and migratory effector memory T-cells. Both memory populations are the first adaptive immune cells recruited to sites of infection/inflammation. Effector memory CD8+ T-cells have been shown to be important as a first line defense upon re-exposure to pathogens that cause acute infections or replicate in non lymphoid tissues (Bachmann et al., 2005; Huster et al., 2006; Nolz and Harty, 2011). Most of these studies compared recall responses of effector memory with central memory CD8+ T-cells responses using adoptive transfer models. Rapid effector function of effector memory CD8+ T-cells was needed for efficient clearance of the pathogen. The contribution of central memory CD8+ T-cells came later into account, in cases, when infection could not be cleared immediately. With their enhanced proliferation capacity, central memory T-cells offer a reservoir for cytotoxic effector cells, however, with delayed kinetics compared to effector memory cells. Rapid CTL generation against Lysteria monocytogenes (Shedlock et al., 2003), vesicular stomatitis virus (Andreasen et al., 2000) or influenza (Liu et al., 1997) was dependent on CD28 co-stimulation. Therefore CD28 signaling is important in similar infection models

where effector memory CD8+ T-cells provide a better protection than central memory T-cells.

In our data, CD28 signaling was important to sustain the early glycolytic phase. Interestingly, prevention of this early glycolytic phase by either addition of AKT inhibitors or glucose deprivation negatively impacted IFN-γ secretion, which is a well documented effector cytokine for immune function (Dalton et al., 1993). In this context, it is important to differentiate if the early-immediate switch to glycolysis after activation is an exclusive feature of effector memory T-cell or whether this is a common ability among all memory cells. In our study, we compared the metabolic signatures of naïve CD8+ T-cells with effector memory CD8+ T-cells. It is well established that memory T-cells have superior functional capacities compared to naïve, however, the potential impact metabolism plays in the recall response of various memory populations is not yet known. An important next step will be to compare metabolic features between different memory subsets. Unfortunately, we have not been able to do this due to technical limitations. The XF24 flux analyzer requires a significant amount of cells to be plated per well and there was insufficient central memory T-cells in peripheral blood to perform metabolic measurements (see also **supplementary FigureS1**). However, further characterization of metabolic profiles of memory T-cells with better technologies, such as the XF96 analyzer, will allow us to further dissect the underlying biology of the early-glycolytic phase in effector memory T-cells.

Glucose availability can modulate immune responses. Recently it has been shown that low dose 2-DG treatment (1mM) only inhibited glycolysis slightly but significantly impaired in vitro differentiation of Th1, Th2 and Th17 cells and promoted Treg induction. Using a transfer model of EAE, pretreatment of the cells with 2-DG significantly reduced the ability of TH17 cells to cause EAE (Shi et al., 2011). Low glucose levels are sufficient for IFN-γ production. Effector memory CD8+ T-cells that were activated in glucose free medium but supplemented with 10% serum had lower glucose supply compared to cells in glucose containing medium. However, this low glucose concentration of about 0.5 mM was enough to promote normal IFN-γ production. This is in line with earlier studies reporting no impairment of survival and only slight impairment of proliferation (48h) with 0.5 mM glucose present in the medium (Maciver et al., 2008). Additional treatment with 10 mM 2-DG, creating a molar ratio (2-DG/glucose) of 20:1, nearly blocked IFN-γ production compared to complete glucose free conditions. The residual production might occur due to an incomplete inhibition of glycolysis since in previous studies 2-DG/glucose ratios of 25:1 have been required to completely block CTL mediated cytolysis (MacDonald, 1977).

Several findings in our study have been demonstrated earlier in primary CD8+ T-cell immune response. Similar to our data, CD69 upregulation following activation was not affected by glucose deprivation (Wang et al., 2011), however, glucose has been shown to be important for IFN-γ production in effector T-cells (Cham and Gajewski, 2005a). Our data extend this knowledge to human effector memory CD8+ T-cells offering potentially new strategies to modulate local recall responses.

III. Critical points

The Seahorse XF24 flux analyzer measures small pH changes in the medium. For this reason, all the experiments have to be performed in unbuffered serum free medium. The absence of serum might be an important factor influencing the metabolic responsiveness of CD8+ T-cells. Additionally, the metabolic flux analyzer operates at 21% oxygen partial pressure as most other *in vitro* culture systems. Several studies have revealed that oxygen pressure is much lower in lymph nodes and spleen (Caldwell et al., 2001). How more physiologic levels of oxygen will impact the metabolic capacities of different T-cell subsets is unknown.

In several described experiments, naïve and effector memory CD8+ T-cells were activated with soluble mABs. When serum was present prior to antibody injection, serum significantly blocked CD8+ T-cell activation. Adding the serum 3 hours after activation circumvented this problem. Still, at the moment of activation, no serum was present. However, activation in the presence of serum was still achieved by using beads coupled with αCD3/CD28. Since we were interested in the possible impact of early glycolytic switch on immune function, we chose to mimic the "in Seahorse" activation conditions as much as possible.

Low glucose levels (0.5 mM) were sufficient to completely restore IFN-γ production. To achieve complete glucose deprivation we either used 10 mM 2-DG or activated T-cells in the absence of serum. Both approaches resulted in a complete inhibition of IFN-γ production but not CD69 upregulation. A more elegant way to directly address the impact of glucose on IFN-γ production is to dialyze out glucose from human AB serum.

PERSPECTIVES

Gene expression is not only regulated by transcription factors, but also by epigenetic modifications. Open chromatin allows gene transcription, whereas heterochromatin minimizes transcription. Specific modifications of histones influence the actual or potential transcriptional state (Jenuwein and Allis, 2001). Several studies in human and mouse T-cells have described genes that were equally expressed in resting naïve and memory CD8+ T-cells, upon activation however, transcription was much greater in the memory cells compared to activated naïve T-cells. These genes are *poised* for activation-induced rapid transcription because of their higher histone acetylation (Araki et al., 2008; Fann et al., 2006). More importantly, these genes are closely linked to effector function, such as IFN-γ or chemokine receptors. In addition, epigenetic modifications can be inherited stably from a cell to its descendants (Fitzpatrick et al., 1999) having the potential therefore to transmit memory during homeostatic proliferation. A second epigenetic mechanism of gene silencing is DNA methylation (Bird and Wolffe, 1999). DNA is typically methylated on CpG islands. Interestingly, 70% of gene promoters are associated with CpG islands (Saxonov et al., 2006). IFN-γ secretion is critical for the immune function of CD8+ T-cells (Dalton et al., 1993). In naïve CD8+ T-cells, several CpG sites in the promoter are methylated (Fitzpatrick et al., 1998). Upon activation, the IFN-γ promoter is de-methylated and again partly methylated in memory cells (Kersh et al., 2006). However, upon reactivation the promoter was rapidly de-methylated in effector memory CD8+ T-cells resulting in increased IFN-γ production. Although a DNA de-methylase enzyme has not been identified, this rapid de-methylation was independent of proliferation. Interestingly, the IL2 promoter was also demethylated after activation in effector T-cells but remained demethylated in memory T-cells. In the same study, the authors also observed that memory cells that have been treated with DNA synthesis inhibitors did not affect IFN-γ transcription as measured by IFN-γ mRNA and protein expression levels. Interestingly, but not discussed in their study, treatment of effector memory CD8+ T-cells with cycloheximide,

a protein synthesis inhibitor, also affected IFN-γ mRNA levels. In addition, actinomycin-D, a transcription inhibitor only had minimal effects on early IFN-γ production. Another independent study reported similar findings (Cham and Gajewski, 2005a). In this study, glucose availability was important for effector CD8+ T-cells to produce IFN-γ. Adding cycloheximide at early timepoints (2-6h) inhibited IFN-γ transcription, whereas addition at later timepoints did not alter IFN-γ mRNA levels. IL2 transcription was not affected at any timepoint. The authors concluded that, a de novo protein must be produced within the first hours after activation for an efficient transcription of IFN-γ.

Our data shows also shows a dependency on glucose for IFN-γ production in effector memory T-cells. The two mechanisms, rapid demethylation of the IFN-γ promoter and increased glycolytic flux are potentially linked in memory CD8+ T-cells. For future studies, it will be interesting to address the importance of early-immediate glycolytic phase for IL2 production, since the promoter for this cytokine is completely demethylated in the effector and memory subset (Kersh et al., 2006) and was less affected by glucose deprivation in effector CD8+ T-cells (Cham and Gajewski, 2005a). In addition, it has to be evaluated if glucose deprivation affects the rapid demethylation on the IFN-γ promoter. In summary, the primed glycolytic capacity in effector memory cells could potentially be an indispensable requirement for transcription of poised genes, such as IFN-γ.

Recent progress in understanding the molecular inter-connectivity between cellular metabolic states and epigenetic modifications has revealed mechanisms on how metabolic flux can effect gene transcription (Locasale and Cantley, 2011; Lu and Thompson, 2012). Most chromatin modifying enzymes require cofactors or substrates that are intermediates in the metabolic pathways. As an example, cytosolic acetyl-CoA -the main substrate for histone acetylation- comes from citrate that has been exported from the mitochondria via ATP-citrate lyase (ACL). Citrate itself can be produced via glycolysis or glutaminolyis. Tracing experiments with C13 labeled glucose in cells with activated Myc have shown that

half of the acetyl groups on H4K16 came from glucose-derived acetyl-CoA (Morrish et al. 2010). Activated T-cells increase glucose and glutamine uptake simultaneously. This increase in glutamine uptake is thought to replenish the citrate that has been used for biosynthesis. In the epigenetic context however, this uptake is also likely to be important for transcription regulation. Highly proliferating cells produce ATP via aerobic glycolyis. The conversion of pyruvate to lactate is not only regenerating NAD+ needed for continuous flux in the glycolytic pathway, but also to generate a positive oxidative redox potential (high NAD+/NADH ratio). Interestingly, NAD+ is an important stimulatory cofactor for the deacetylase SIRT1 (Locasale and Cantley, 2011). Regulation of SIRT1 activity by glycolytic flux is potentially another pathway that can control the expression of poised effector genes. Further studies will have to be done to address the importance of metabolic flux in the regulation of immune functions.
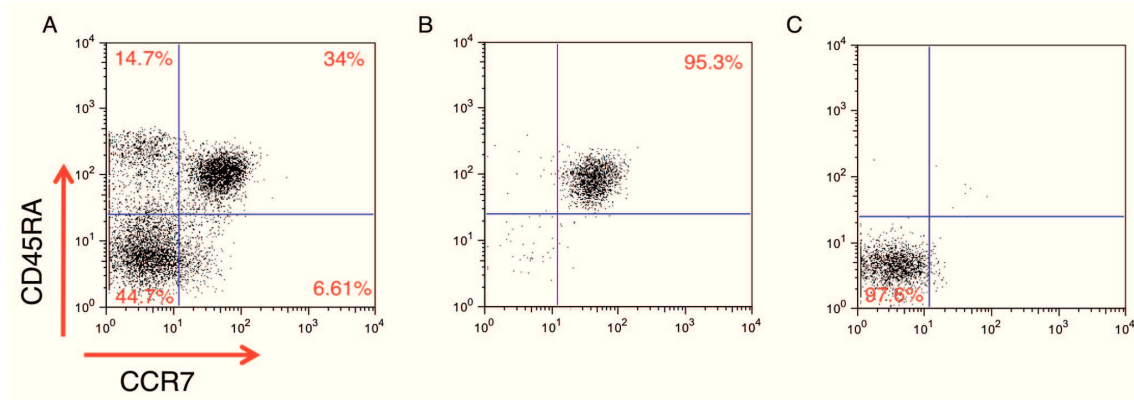
Figure S1. Sorting strategy for CD8+ T-cell subpopulations.

(**A**) Representative dot plot of fresh isolated CD8+ T-cells stained for CD45RA and CCR7. Four CD8+ T-cell subpopulations are identified as follows: naïve (NV, CCR7+CD45RA+), central memory (CM, CCR7+CD45RA^{neg}), effector memory (EM, CCR7^{neg}CD45RA^{neg}) and EMRA (CD45RA re-expressing effector memory, CCR7^{neg}CD45RA+). Values represent frequency of total gated events.

(**B**, **C**) Representative dot plots of naïve (**B**) and effector memory (**C**) CD8+ T-cell subsets sorted by FACS (purity always greater than 95%). Values represent frequency of total gated events.
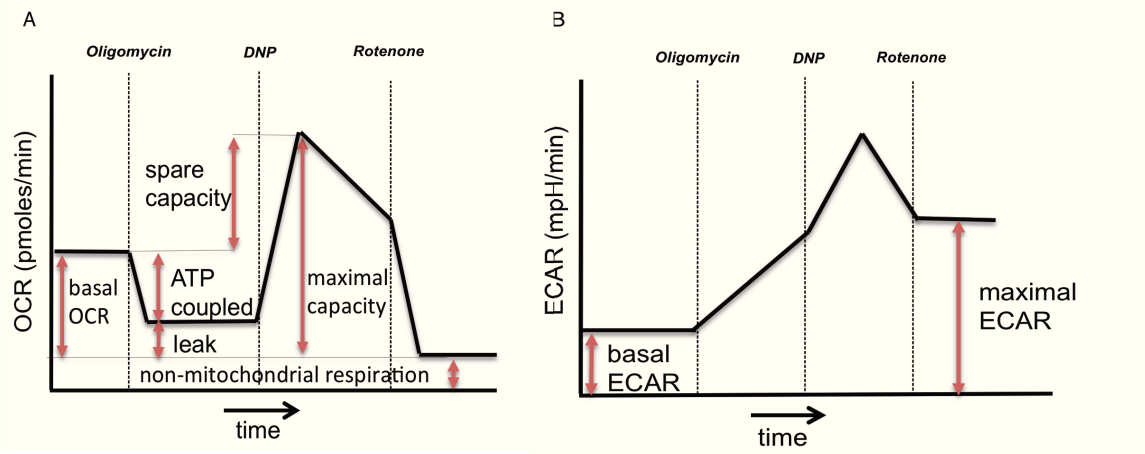
Figure S2. Diagram of OCR and ECAR profiles generated by the Seahorse extracellular flux analyzer.

(**A**) Representative OCR time course under basal conditions and following perturbation of mitochondrial respiration with oligomycin (1 μM), DNP (175 μM) and rotenone (1 μM). Using this perturbation profiling technique, four OCR rates are directly measured by the instrument: the non-corrected basal OCR [$OCR_{(basal-nc)}$], the rate following inhibition of ATP synthase [$OCR_{(oligomycin)}$], the peak rate following mitochondrial uncoupling [$OCR_{(peak-DNP)}$], and the rate following inhibition of mitochondrial respiration [$OCR_{(rotenone)}$]. The following respiratory parameters (indicated by red double-ended arrows in the diagram) are calculated using the formulas below:

(1) basal respiration = [$OCR_{(basal-nc)}$] – [$OCR_{(rotenone)}$]
(2) ATP coupled respiration = [$OCR_{(basal-nc)}$] – [$OCR_{(oligomycin)}$]
(3) leak respiration = [$OCR_{(oligomycin)}$] – [$OCR_{(rotenone)}$]
(4) maximal respiratory capacity = [$OCR_{(peak-DNP)}$] – [$OCR_{(rotenone)}$]
(5) spare respiratory capacity = [$OCR_{(peak-DNP)}$] – [$OCR_{(basal-nc)}$]
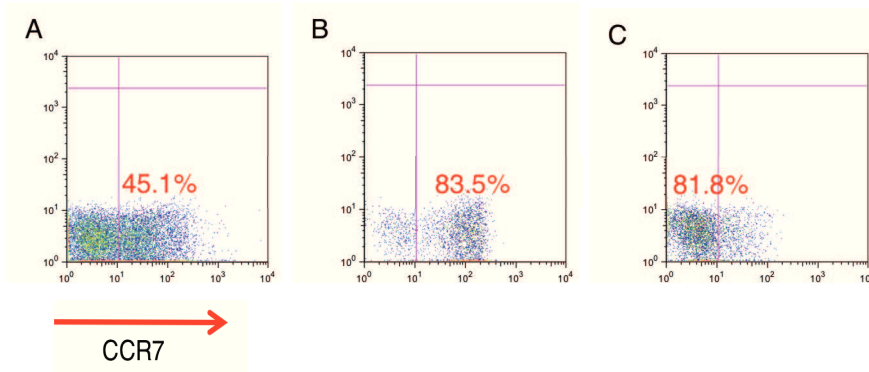(6) non-mitochondrial respiration = $OCR_{(rotenone)}$

Figure S3. Sorting strategy for CD8+ T-cells used in palmitate oxidation assays.

(**A-C**) CD8+ T-cells were sorted according to CCR7 expression as described in the materials and methods section. Representative dot plots of (A) CCR7-PE stained, pre-sorted CD8+ T-cells, and post-sorted CCR7+ (B), and CCR7^{neg} (C) fractions are shown. Sort purity of both fractions used in all palmitate oxidation experiments was >80%.
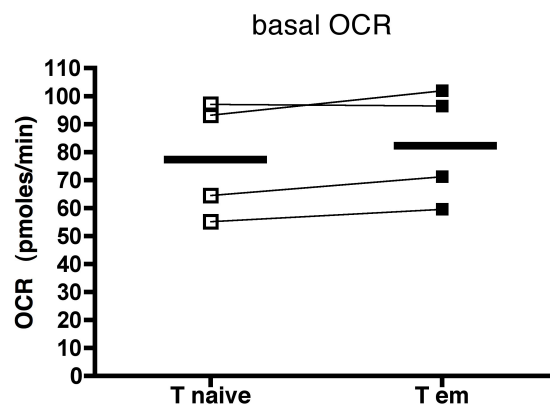

Figure S4. Basal OCR of naïve and effector memory CD8+ T-cells remains similar in the absence of glucose.

The basal OCR of naïve (open square) and effector memory (closed squares) CD8+ T-cells were determined in glucose free RPMI using the extracellular flux analyzer. Sorting and experimental techniques are described in the materials and method section. Data from 4 donors and mean values are shown.
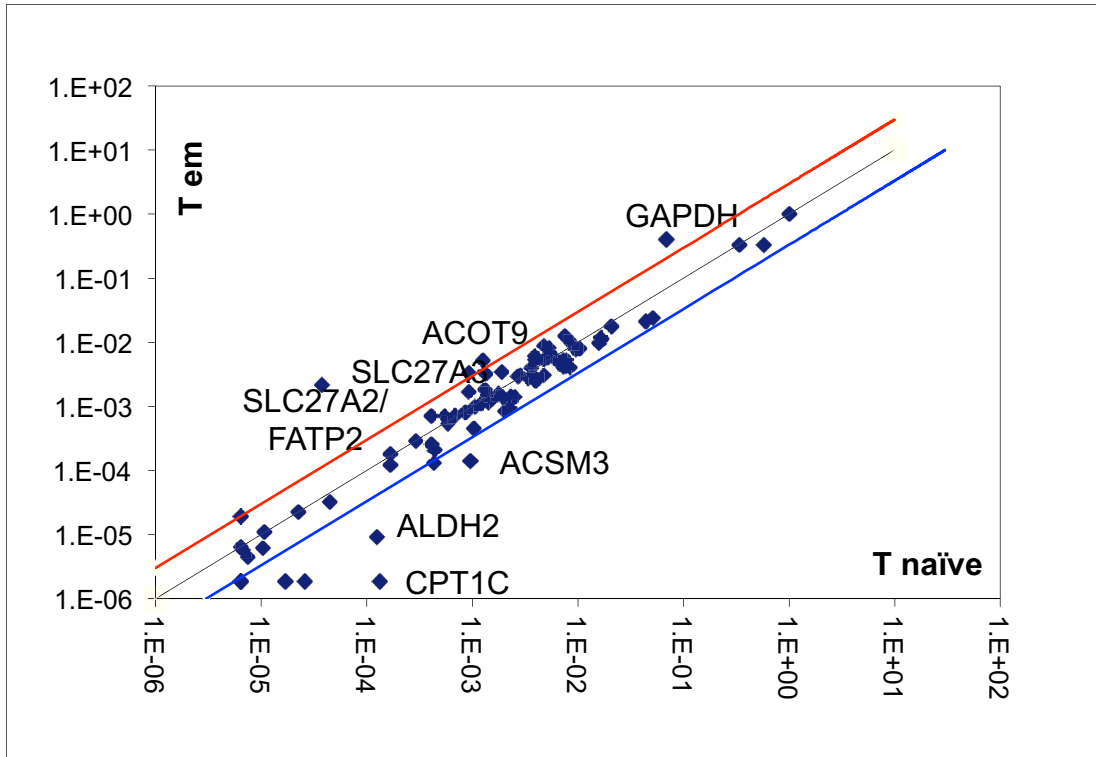
Figure S5. Lipid metabolism gene-expression profiling in naïve and effector memory CD8+ T-cells.

To compare lipid metabolism gene expression between naïve and effector memory CD8+ T-cells, the Fatty Acid Metabolism PCR Array from SA Bioscience (Qiagen) was used according to the manufacturer's protocol. Total RNA was isolated as described in the EXPERIMENTAL PROCEDURES section. The red and blue lines indicate a three-fold increase. Genes left of the red line are at least three fold higher expressed in effector memory cells than in naïve CD8+ T-cells. Genes located on the right of the blue line are down-regulated in the effector memory subset compared to the naïve CD8+ T-cells.
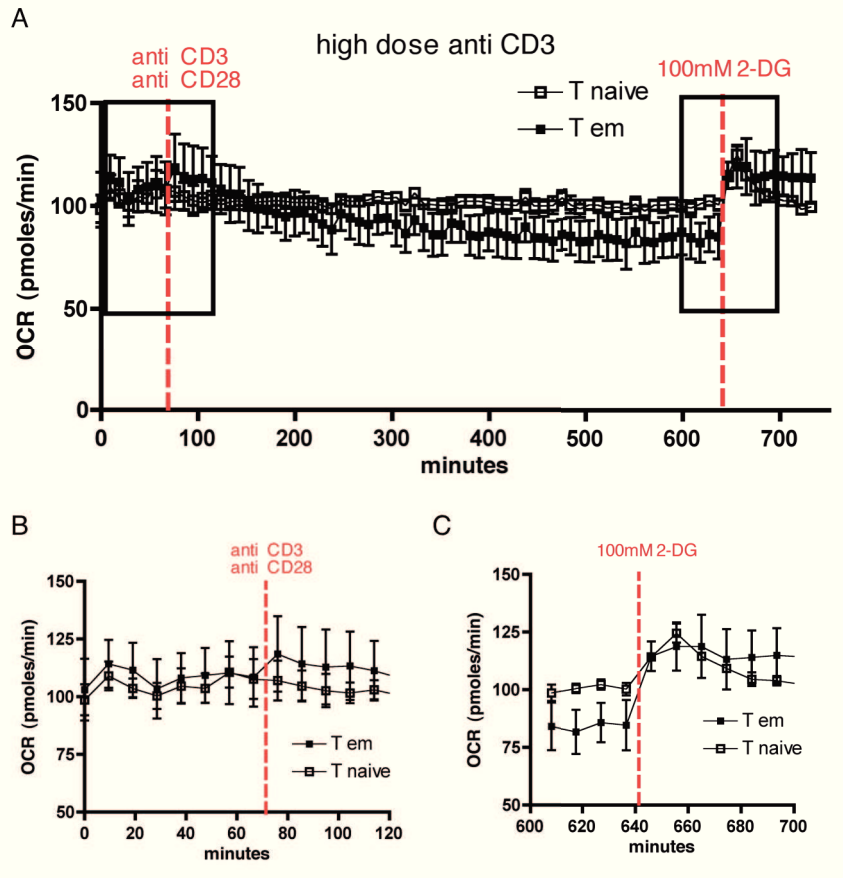
Figure S6. Polyclonal activation does not impact the OCR of naïve and effector memory CD8+ T-cells.

(**A**) OCR time course of naïve (open square) and effector memory (close square) CD8+ T-cells following 'in-Seahorse' polyclonal activation. As described in the material and methods section, cells were treated with anti-CD3 and anti-CD28 mAb, and OCR measured pre- and post-activation, and following treatment with 2-deoxy D-glucose (2-DG) (100 mM).

(**B**, **C**) Magnified sections (black boxes in Figure S6A) of the OCR profile of both naïve and effector memory subpopulations following (**B**) antibody and (**C**) 2-DG treatments. Anti-CD3 and anti-CD28 mAb injection does not alter the OCR. Injection of 2-DG leads to an immediate decrease in ECAR (**Figure 15B**), and to a compensatory increase in OCR.
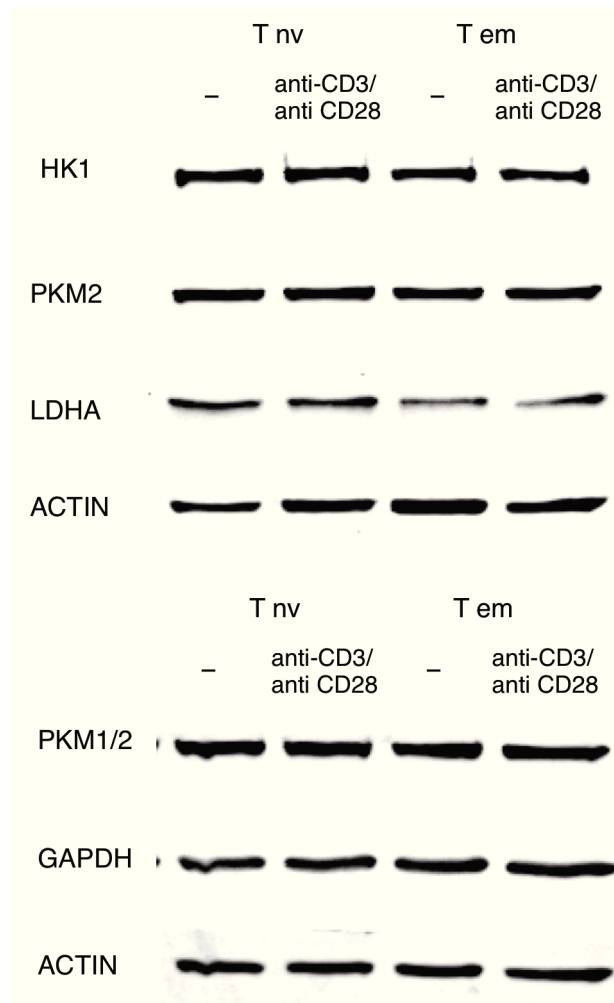
Figure S7. Protein expression of glycolytic enzymes in naïve and effector memory CD8+ T-cells remains unchanged after early activation.

Fresh-isolated CD8+ T-cell subsets were activated with αCD3 and αCD28 mAb for 3 hours. Whole cell lysates from non-activated and activated cells were then probed for HK1, GAPDH, PKM2, PKM1/2 and LDHA expression by immunoblotting. Actin was used as the loading control. Results from 1 of 2 independently assessed donors are shown.
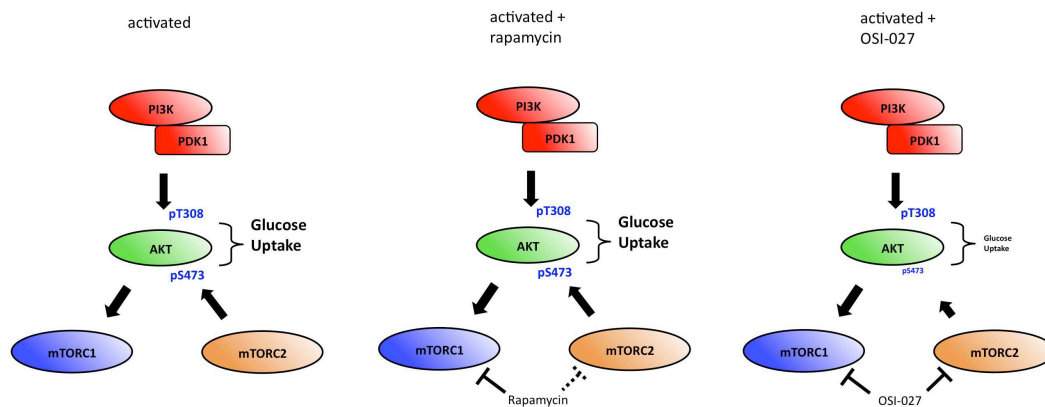
Figure S8. Model explaining the different effects of rapamycin and OSI-027 on immediate-early glycolytic switch

Phosphorylation of both sites fully activate AKT and promotes glucose uptake (left). Rapamycin (20 ng/ml) only blocks mTORC1 and both sites on AKT are still phosphorylated upon T-cell activation (middle). Treatment with OSI-027 efficently blocks both mTOR complexes with a consequent reduction of phosphorylation on serine 473 (right). AKT is not fully activated and glucose uptake is decreased.

REFERENCES

Adachi, K., and Davis, M.M. (2011). T-cell receptor ligation induces distinct signaling pathways in naive vs. antigen-experienced T cells. Proceedings of the National Academy of Sciences of the United States of America *108*, 1549-1554.

Allam, A., Conze, D.B., Giardino Torchia, M.L., Munitic, I., Yagita, H., Sowell, R.T., Marzo, A.L., and Ashwell, J.D. (2009). The CD8+ memory T-cell state of readiness is actively maintained and reversible. Blood *114*, 2121-2130.

Andreasen, S.O., Christensen, J.E., Marker, O., and Thomsen, A.R. (2000). Role of CD40 ligand and CD28 in induction and maintenance of antiviral CD8+ effector T cell responses. Journal of immunology *164*, 3689-3697.

Araki, K., Turner, A.P., Shaffer, V.O., Gangappa, S., Keller, S.A., Bachmann, M.F., Larsen, C.P., and Ahmed, R. (2009). mTOR regulates memory CD8 T-cell differentiation. Nature *460*, 108-112.

Araki, Y., Fann, M., Wersto, R., and Weng, N.P. (2008). Histone acetylation facilitates rapid and robust memory CD8 T cell response through differential expression of effector molecules (eomesodermin and its targets: perforin and granzyme B). Journal of immunology *180*, 8102-8108.

Bachmann, M.F., Wolint, P., Schwarz, K., and Oxenius, A. (2005). Recall Proliferation Potential of Memory CD8 + T Cells and Antiviral Protection. Journal of Immunolgy *175*, 4677-4685.

Badovinac, V.P., Haring, J.S., and Harty, J.T. (2007). Initial T cell receptor transgenic cell precursor frequency dictates critical aspects of the CD8(+) T cell response to infection. Immunity *26*, 827-841.

Baixauli, F., Martin-Cofreces, N.B., Morlino, G., Carrasco, Y.R., Calabia-Linares, C., Veiga, E., Serrador, J.M., and Sanchez-Madrid, F. (2011). The mitochondrial fission factor dynamin-related protein 1 modulates T-cell receptor signalling at the immune synapse. The EMBO journal *30*, 1238-1250.

Bental, M., and Deutsch, C. (1993). Metabolic Changes in Activated T Cells: An NMR Study of Human Peripheral Blood Lymphocytes. Magn. Reson. Med. *29*, 317-326.

Bevan, M.J. (2011). Memory T cells as an occupying force. European journal of immunology *41*, 1192-1195.

Bird, A.P., and Wolffe, A.P. (1999). Methylation-induced repression--belts, braces, and chromatin. Cell *99*, 451-454.

Borowski, A.B., Boesteanu, A.C., Mueller, Y.M., Carafides, C., Topham, D.J., Altman, J.D., Jennings, S.R., and Katsikis, P.D. (2007). Memory CD8+ T cells require CD28 costimulation. Journal of immunology *179*, 6494-6503.

Brand, M.D., and Nicholls, D.G. (2011). Assessing mitochondrial dysfunction in cells. The Biochemical journal *435*, 297-312.

Brunn, G.J., Williams, J., Sabers, C., Wiederrecht, G., Lawrence, J.C., Jr., and Abraham, R.T. (1996). Direct inhibition of the signaling functions of the mammalian target of

rapamycin by the phosphoinositide 3-kinase inhibitors, wortmannin and LY294002. The EMBO journal *15*, 5256-5267.

Buentke, E., Mathiot, A., Tolaini, M., Di Santo, J., Zamoyska, R., and Seddon, B. (2006). Do CD8 effector cells need IL-7R expression to become resting memory cells? Blood *108*, 1949-1956.

Caldwell, C.C., Kojima, H., Lukashev, D., Armstrong, J., Farber, M., Apasov, S.G., and Sitkovsky, M.V. (2001). Differential effects of physiologically relevant hypoxic conditions on T lymphocyte development and effector functions. Journal of immunology *167*, 6140-6149.

Capasso, M., Bhamrah, M.K., Henley, T., Boyd, R.S., Langlais, C., Cain, K., Dinsdale, D., Pulford, K., Khan, M., Musset, B*., et al.* (2010). HVCN1 modulates BCR signal strength via regulation of BCR-dependent generation of reactive oxygen species. Nature immunology *11*, 265-272.

Cham, C.M., Driessens, G., O'Keefe, J.P., and Gajewski, T.F. (2008). Glucose deprivation inhibits multiple key gene expression events and effector functions in CD8+ T cells. European journal of immunology *38*, 2438-2450.

Cham, C.M., and Gajewski, T.F. (2005a). Glucose availability regulates IFN-gamma production and p70S6 kinase activation in CD8+ effector T cells. Journal of immunology *174*, 4670-4677.

Cham, C.M., and Gajewski, T.F. (2005b). Glucose Availability Regulates IFN-γ Production and p70S6 Kinase Activation in CD8+ Effector T Cells. Journal of Immunolgy *174*, 4670-4677.

Champagne, P., Ogg, G.S., King, A.S., Knabenhans, C., Ellefsen, K., Nobile, M., Appay, V., Rizzardi, G.P., Fleury, S., Lippk, M*., et al.* (2001). Skewed maturation of memory HIV-specfic CD8 T lymphocytes. Nature *410*, 106-111.

Colombetti, S., Basso, V., Mueller, D.L., and Mondino, A. (2006). Prolonged TCR/CD28 Engagement Drives IL-2-Independent T Cell Clonal Expansion through Signaling Mediated by the Mammalian Target of Rapamycin. Journal of Immunolgy *176*, 2730-2738.

Cui, W., and Kaech, S.M. (2010). Generation of effector CD8+ T cells and their conversion to memory T cells. Immunological Reviews *236*, 151-166.

Curtsinger, J.M., and Mescher, M.F. (2010). Inflammatory cytokines as a third signal for T cell activation. Current opinion in immunology *22*, 333-340.

D'Souza, A.D., Parikh, N., Kaech, S.M., and Shadel, G.S. (2007). Convergence of multiple signaling pathways is required to coordinately up-regulate mtDNA and mitochondrial biogenesis during T cell activation. Mitochondrion *7*, 374-385.

Dalton, D.K., Pitts-Meek, S., Keshav, S., Figari, I.S., Bradley, A., and Stewart, T.A. (1993). Multiple defects of immune cell function in mice with disrupted interferon-gamma genes. Science *259*, 1739-1742.

Delgoffe, G.M., Pollizzi, K.N., Waickman, A.T., Heikamp, E., Meyers, D.J., Horton, M.R., Xiao, B., Worley, P.F., and Powell, J.D. (2011). The kinase mTOR regulates the differentiation of helper T cells through the selective activation of signaling by mTORC1 and mTORC2. Nature immunology *12*, 295-303.

Delgoffe, G.M., and Powell, J.D. (2009). mTOR: taking cues from the immune microenvironment. Immunology *127*, 459-465.

Falcon, A., Doege, H., Fluitt, A., Tsang, B., Watson, N., Kay, M.A., and Stahl, A. (2010). FATP2 is a hepatic fatty acid transporter and peroxisomal very long-chain acyl-CoA synthetase. American journal of physiology. Endocrinology and metabolism *299*, E384-393.

Fann, M., Godlove, J.M., Catalfamo, M., Wood, W.H., 3rd, Chrest, F.J., Chun, N., Granger, L., Wersto, R., Madara, K., Becker, K*., et al.* (2006). Histone acetylation is associated with differential gene expression in the rapid and robust memory CD8(+) T-cell response. Blood *108*, 3363-3370.

Finlay, D.K., Rosenzweig, E., Sinclair, L.V., Feijoo-Carnero, C., Hukelmann, J.L., Rolf, J., Panteleyev, A.A., Okkenhaug, K., and Cantrell, D.A. (2012). PDK1 regulation of mTOR and hypoxia-inducible factor 1 integrate metabolism and migration of CD8+ T cells. The Journal of experimental medicine *209*, 2441-2453.

Fitzpatrick, D.R., Shirley, K.M., and Kelso, A. (1999). Cutting edge: stable epigenetic inheritance of regional IFN-gamma promoter demethylation in CD44highCD8+ T lymphocytes. Journal of immunology *162*, 5053-5057.

Fitzpatrick, D.R., Shirley, K.M., McDonald, L.E., Bielefeldt-Ohmann, H., Kay, G.F., and Kelso, A. (1998). Distinct methylation of the interferon gamma (IFN-gamma) and interleukin 3 (IL-3) genes in newly activated primary CD8+ T lymphocytes: regional IFN-gamma promoter demethylation and mRNA expression are heritable in CD44(high)CD8+ T cells. The Journal of experimental medicine *188*, 103-117.

Fox, C.J., Hammerman, P.S., and Thompson, C.B. (2005). Fuel feeds function: energy metabolism and the T-cell response. Nature reviews. Immunology *5*, 844-852.

Frauwirth, K.A., Riley, J.L., Harris, M.H., Parry, R.V., Rathmell, J.C., Plas, D.R., Elstrom, R.L., June, C.H., and Thompson, C.B. (2002a). The CD28 signaling pathway regulates glucose metabolism. Immunity *16*, 769-777.

Frauwirth, K.A., Riley, J.L., Harris, M.H., Parry, R.V., Rathmell, J.C., Plas, D.R., Elstrom, R.L., June, C.H., and Thompson, C.B. (2002b). The CD28 Signaling Pathway Regulates Glucose Metabolism. Immunity *16*, 769-777.

Gan, X., Wang, J., Su, B., and Wu, D. (2011). Evidence for direct activation of mTORC2 kinase activity by phosphatidylinositol 3,4,5-trisphosphate. The Journal of biological chemistry *286*, 10998-11002.

Gebhardt, T., Wakim, L.M., Eidsmo, L., Reading, P.C., Heath, W.R., and Carbone, F.R. (2009). Memory T cells in nonlymphoid tissue that provide enhanced local immunity during infection with herpes simplex virus. Nature immunology *10*, 524-530.

Geginat, J., Lanzavecchia, A., and Sallusto, F. (2003). Proliferation and differentiation potential of human CD8+ memory T-cell subsets in response to antigen or homeostatic cytokines. Blood *101*, 4260-4266.

Gergely, P., Jr., Niland, B., Gonchoroff, N., Pullmann, R., Jr., Phillips, P.E., and Perl, A. (2002). Persistent mitochondrial hyperpolarization, increased reactive oxygen intermediate production, and cytoplasmic alkalinization characterize altered IL-10 signaling in patients with systemic lupus erythematosus. J Immunol *169*, 1092-1101.

Gerlach, C., van Heijst, J.W., Swart, E., Sie, D., Armstrong, N., Kerkhoven, R.M., Zehn, D., Bevan, M.J., Schepers, K., and Schumacher, T.N. (2010). One naive T cell, multiple fates in CD8+ T cell differentiation. The Journal of experimental medicine *207*, 1235-1246.

Greiner, E.F., Guppy, M., and Brand, K. (1994). Glucose is essential for proliferation and the glycolytic enzyme induction that provokes a transition to glycolytic energy production. J Biol Chem *269*, 31484-31490.

Grujic, M., Bartholdy, C., Remy, M., Pinschewer, D.D., Christensen, J.P., and Thomsen, A.R. (2010). The role of CD80/CD86 in generation and maintenance of functional virus-specific CD8+ T cells in mice infected with lymphocytic choriomeningitis virus. Journal of immunology *185*, 1730-1743.

Guertin, D.A., Stevens, D.M., Thoreen, C.C., Burds, A.A., Kalaany, N.Y., Moffat, J., Brown, M., Fitzgerald, K.J., and Sabatini, D.M. (2006). Ablation in mice of the mTORC components raptor, rictor, or mLST8 reveals that mTORC2 is required for signaling to Akt-FOXO and PKCalpha, but not S6K1. Developmental cell *11*, 859-871.

Hansen, S.G., Vieville, C., Whizin, N., Coyne-Johnson, L., Siess, D.C., Drummond, D.D., Legasse, A.W., Axthelm, M.K., Oswald, K., Trubey, C.M.*, et al.* (2009). Effector memory T cell responses are associated with protection of rhesus monkeys from mucosal simian immunodeficiency virus challenge. Nature medicine *15*, 293-299.

Harari, A., Enders, F.B., Cellerai, C., Bart, P.A., and Pantaleo, G. (2009). Distinct profiles of cytotoxic granules in memory CD8 T cells correlate with function, differentiation stage, and antigen exposure. Journal of virology *83*, 2862-2871.

Hardie, D.G. (2007). AMP-activated/SNF1 protein kinases: conserved guardians of cellular energy. Nature reviews. Molecular cell biology *8*, 774-785.

Haring, J.S., Badovinac, V.P., and Harty, J.T. (2006). Inflaming the CD8+ T cell response. Immunity *25*, 19-29.

Harty, J.T., Tvinnereim, A.R., and White, D.W. (2000). CD8+ T cell effector mechanisms in resistance to infection. Annual review of immunology *18*, 275-308.

Hom, J.R., Quintanilla, R.A., Hoffman, D.L., de Mesy Bentley, K.L., Molkentin, J.D., Sheu, S.S., and Porter, G.A., Jr. (2011). The permeability transition pore controls cardiac mitochondrial maturation and myocyte differentiation. Developmental cell *21*, 469-478.

Huster, K.M., Koffler, M., Stemberger, C., Schiemann, M., Wagner, H., and Busch, D.H. (2006). Unidirectional development of CD8+ central memory T cells into protective Listeria-specific effector memory T cells. European journal of immunology *36*, 1453-1464.

Intlekofer, A.M., Takemoto, N., Wherry, E.J., Longworth, S.A., Northrup, J.T., Palanivel, V.R., Mullen, A.C., Gasink, C.R., Kaech, S.M., Miller, J.D.*, et al.* (2005). Effector and memory CD8+ T cell fate coupled by T-bet and eomesodermin. Nature immunology *6*, 1236-1244.

Jacobs, S.R., Herman, C.E., Maciver, N.J., Wofford, J.A., Wieman, H.L., Hammen, J.J., and Rathmell, J.C. (2008). Glucose uptake is limiting in T cell activation and requires CD28-mediated Akt-dependent and independent pathways. Journal of immunology *180*, 4476-4486.

Jameson, S.C., and Masopust, D. (2009). Diversity in T cell memory: an embarrassment of riches. Immunity *31*, 859-871.

Jenuwein, T., and Allis, C.D. (2001). Translating the histone code. Science *293*, 1074-1080.

Jiang, X., Clark, R.A., Liu, L., Wagers, A.J., Fuhlbrigge, R.C., and Kupper, T.S. (2012). Skin infection generates non-migratory memory CD8+ T(RM) cells providing global skin immunity. Nature *483*, 227-231.

Jones, R.G., and Thompson, C.B. (2007). Revving the engine: signal transduction fuels T cell activation. Immunity *27*, 173-178.

Joshi, N.S., Cui, W., Chandele, A., Lee, H.K., Urso, D.R., Hagman, J., Gapin, L., and Kaech, S.M. (2007). Inflammation directs memory precursor and short-lived effector CD8(+) T cell fates via the graded expression of T-bet transcription factor. Immunity *27*, 281-295.

Kaech, S.M., Tan, J.T., Wherry, E.J., Konieczny, B.T., Surh, C.D., and Ahmed, R. (2003). Selective expression of the interleukin 7 receptor identifies effector CD8 T cells that give rise to long-lived memory cells. Nature immunology *4*, 1191-1198.

Kersh, E.N., Fitzpatrick, D.R., Murali-Krishna, K., Shires, J., Speck, S.H., Boss, J.M., and Ahmed, R. (2006). Rapid demethylation of the IFN-gamma gene occurs in memory but not naive CD8 T cells. Journal of immunology *176*, 4083-4093.

Koopman, W.J., Verkaart, S., van Emst-de Vries, S.E., Grefte, S., Smeitink, J.A., and Willems, P.H. (2006). Simultaneous quantification of oxidative stress and cell spreading using 5-(and-6)-chloromethyl-2',7'-dichlorofluorescein. Cytometry. Part A : the journal of the International Society for Analytical Cytology *69*, 1184-1192.

Kopf, H., de la Rosa, G.M., Howard, O.M., and Chen, X. (2007). Rapamycin inhibits differentiation of Th17 cells and promotes generation of FoxP3+ T regulatory cells. International immunopharmacology *7*, 1819-1824.

Kornberg, M.D., Sen, N., Hara, M.R., Juluri, K.R., Nguyen, J.V., Snowman, A.M., Law, L., Hester, L.D., and Snyder, S.H. (2010). GAPDH mediates nitrosylation of nuclear proteins. Nature cell biology *12*, 1094-1100.

Laplante, M., and Sabatini, D.M. (2012). mTOR signaling in growth control and disease. Cell *149*, 274-293.

Liu, X., Wang, X., Zhang, J., Lam, E.K., Shin, V.Y., Cheng, A.S., Yu, J., Chan, F.K., Sung, J.J., and Jin, H.C. (2010). Warburg effect revisited: an epigenetic link between glycolysis and gastric carcinogenesis. Oncogene *29*, 442-450.

Liu, Y., Wenger, R.H., Zhao, M., and Nielsen, P.J. (1997). Distinct costimulatory molecules are required for the induction of effector and memory cytotoxic T lymphocytes. The Journal of experimental medicine *185*, 251-262.

Locasale, J.W., and Cantley, L.C. (2011). Metabolic flux and the regulation of mammalian cell growth. Cell metabolism *14*, 443-451.

Lu, C., and Thompson, C.B. (2012). Metabolic regulation of epigenetics. Cell metabolism *16*, 9-17.

MacDonald, H.R. (1977). Energy metabolism and T-cell-mediated cytolysis. II. Selective inhibition of cytolysis by 2-deoxy-D-glucose. The Journal of experimental medicine *146*, 710-719.

Macintyre, A.N., Finlay, D., Preston, G., Sinclair, L.V., Waugh, C.M., Tamas, P., Feijoo, C., Okkenhaug, K., and Cantrell, D.A. (2011). Protein kinase B controls transcriptional programs that direct cytotoxic T cell fate but is dispensable for T cell metabolism. Immunity *34*, 224-236.

MacIver, N.J., Blagih, J., Saucillo, D.C., Tonelli, L., Griss, T., Rathmell, J.C., and Jones, R.G. (2011). The liver kinase B1 is a central regulator of T cell development, activation, and metabolism. Journal of immunology *187*, 4187-4198.

Maciver, N.J., Jacobs, S.R., Wieman, H.L., Wofford, J.A., Coloff, J.L., and Rathmell, J.C. (2008). Glucose metabolism in lymphocytes is a regulated process with significant effects on immune cell function and survival. Journal of leukocyte biology *84*, 949-957.

Maciver, N.J., Michalek, R.D., and Rathmell, J.C. (2013). Metabolic Regulation of T Lymphocytes. Annual review of immunology.

Marzo, A.L., Klonowski, K.D., Le Bon, A., Borrow, P., Tough, D.F., and Lefrancois, L. (2005). Initial T cell frequency dictates memory CD8+ T cell lineage commitment. Nature immunology *6*, 793-799.

Masopust, D., Ha, S.-J., Vezys, V., and Ahmed, R. (2006). Stimulation History Dictates Memory CD8 T Cell Phenotype: Implications for Prime-Boost Vaccination. Journal of Immunolgy *177*, 831-839.

Masopust, D., and Picker, L.J. (2012). Hidden memories: frontline memory T cells and early pathogen interception. Journal of immunology *188*, 5811-5817.

Maus, M.V., Kovacs, B., Kwok, W.W., Nepom, G.T., Schlienger, K., Riley, J.L., Allman, D., Finkel, T.H., and June, C.H. (2004). Extensive replicative capacity of human central memory T cells. Journal of immunology *172*, 6675-6683.

Mazzola, J.L., and Sirover, M.A. (2003). Subcellular localization of human glyceraldehyde-3-phosphate dehydrogenase is independent of its glycolytic function. Biochimica et biophysica acta *1622*, 50-56.

Mescher, M.F., Curtsinger, J.M., Agarwal, P., Casey, K.A., Gerner, M., Popescu, C.D.H.F., and Xiao, Z. (2006). Signals required for programming effector and memory development by CD8+ T cells. Immunological Reviews *211*, 81-92.

Michalek, R.D., Gerriets, V.A., Jacobs, S.R., Macintyre, A.N., MacIver, N.J., Mason, E.F., Sullivan, S.A., Nichols, A.G., and Rathmell, J.C. (2011). Cutting edge: distinct glycolytic and lipid oxidative metabolic programs are essential for effector and regulatory CD4+ T cell subsets. Journal of immunology *186*, 3299-3303.

Mills, R.E., and Jameson, J.M. (2009). T cell dependence on mTOR signaling. Cell Cycle *8*, 545-548.

Nolz, J.C., and Harty, J.T. (2011). Protective capacity of memory CD8+ T cells is dictated by antigen exposure history and nature of the infection. Immunity *34*, 781-793.

Pearce, E.L., and Shen, H. (2007). Generation of CD8 T Cell Memory Is Regulated by IL-12. Journal of Immunolgy *179*, 2074-2081.

Pearce, E.L., Walsh, M.C., Cejas, P.J., Harms, G.M., Shen, H., Wang, L.S., Jones, R.G., and Choi, Y. (2009). Enhancing CD8 T-cell memory by modulating fatty acid metabolism. Nature *460*, 103-107.

Petrovas, C., Mueller, Y.M., Dimitriou, I.D., Altork, S.R., Banerjee, A., Sklar, P., Mounzer, K.C., Altman, J.D., and Katsikis, P.D. (2007). Increased mitochondrial mass characterizes the survival defect of HIV-specific CD8(+) T cells. Blood *109*, 2505-2513.

Pihlgren, M., Dubois, P.M., Tomkowiak, M., Sjogren, T., and Marvel, J. (1996). Resting memory CD8+ T cells are hyperreactive to antigenic challenge in vitro. The Journal of experimental medicine *184*, 2141-2151.

Plas, D.R., Rathmell, J.C., and Thompson, C.B. (2002). Homeostatic control of lymphocyte survival: potential origins and implications. Nature immunology *3*, 515-521.

Powell, J.D., and Delgoffe, G.M. (2010). The mammalian target of rapamycin: linking T cell differentiation, function, and metabolism. Immunity *33*, 301-311.

Proud, C.G. (2007). Amino acids and mTOR signalling in anabolic function. Biochemical Society Transactions *35*, 1187-1190.

Rao, R.R., Li, Q., Odunsi, K., and Shrikant, P.A. (2010). The mTOR kinase determines effector versus memory CD8+ T cell fate by regulating the expression of transcription factors T-bet and Eomesodermin. Immunity *32*, 67-78.

Rathmell, J.C., Farkash, E.A., Gao, W., and Thompson, C.B. (2001). IL-7 Enhances the Survival and Maintains the Size of Naive T Cells. Journal of Immunolgy *167*, 6869-6876.

Rathmell, J.C., Vander Heiden, M.G., Harris, M.H., Frauwirth, K.A., and Thompson, C.B. (2000). In the absence of extrinsic signals, nutrient utilization by lymphocytes is insufficient to maintain either cell size or viability. Molecular cell *6*, 683-692.

Rogers, P.R., Dubey, C., and Swain, S.L. (2000). Qualitative changes accompany memory T cell generation: faster, more effective responses at lower doses of antigen. Journal of immunology *164*, 2338-2346.

Romero, P., Zippelius, A., Kurth, I., Pittet, M.J., Touvrey, C., Iancu, E.M., Corthesy, P., Devevre, E., Speiser, D.E., and Rufer, N. (2007). Four functionally distinct populations of human effector-memory CD8+ T lymphocytes. Journal of immunology *178*, 4112-4119.

Sallusto, F., Geginat, J., and Lanzavecchia, A. (2004). Central memory and effector memory T cell subsets: function, generation, and maintenance. Annual review of immunology *22*, 745-763.

Sarkar, S., Kalia, V., Haining, W.N., Konieczny, B.T., Subramaniam, S., and Ahmed, R. (2008). Functional and genomic profiling of effector CD8 T cell subsets with distinct memory fates. The Journal of experimental medicine *205*, 625-640.

Saxonov, S., Berg, P., and Brutlag, D.L. (2006). A genome-wide analysis of CpG dinucleotides in the human genome distinguishes two distinct classes of promoters. Proceedings of the National Academy of Sciences of the United States of America *103*, 1412-1417.

Schluns, K.S., Kieper, W.C., Jameson, S.C., and Lefrançois, L. (2000). Interleukin-7 mediates the homeostasis of naïve and memory CD8 T cells in vivo. Nature immunology *1*, 426-432.

Schwartz, R.H. (2003). T cell anergy. Annual review of immunology *21*, 305-334.

Sharpe, A.H. (2009). Mechanisms of costimulation. Immunological Reviews *229*, 5-11.

Shedlock, D.J., Whitmire, J.K., Tan, J., MacDonald, A.S., Ahmed, R., and Shen, H. (2003). Role of CD4 T cell help and costimulation in CD8 T cell responses during Listeria monocytogenes infection. Journal of immunology *170*, 2053-2063.

Shi, L.Z., Wang, R., Huang, G., Vogel, P., Neale, G., Green, D.R., and Chi, H. (2011). HIF1alpha-dependent glycolytic pathway orchestrates a metabolic checkpoint for the differentiation of TH17 and Treg cells. The Journal of experimental medicine *208*, 1367-1376.

Slifka, M.K., and Whitton, J.L. (2000). Activated and memory CD8+ T cells can be distinguished by their cytokine profiles and phenotypic markers. Journal of immunology *164*, 208-216.

Smith-Garvin, J.E., Koretzky, G.A., and Jordan, M.S. (2009). T cell activation. Annual review of immunology *27*, 591-619.

Soond, D.R., Bjorgo, E., Moltu, K., Dale, V.Q., Patton, D.T., Torgersen, K.M., Galleway, F., Twomey, B., Clark, J., Gaston, J.S.*, et al.* (2010). PI3K p110delta regulates T-cell cytokine production during primary and secondary immune responses in mice and humans. Blood *115*, 2203-2213.

Stemberger, C., Huster, K.M., Koffler, M., Anderl, F., Schiemann, M., Wagner, H., and Busch, D.H. (2007). A single naive CD8+ T cell precursor can develop into diverse effector and memory subsets. Immunity *27*, 985-997.

Takemoto, N., Intlekofer, A.M., Northrup, J.T., Wherry, E.J., and Reiner, S.L. (2006). Cutting Edge: IL-12 Inversely Regulates T-bet and Eomesodermin Expression during Pathogen-Induced CD8+ T Cell Differentiation. Journal of Immunolgy *177*, 7515-7519.

Tamas, P., Hawley, S.A., Clarke, R.G., Mustard, K.J., Green, K., Hardie, D.G., and Cantrell, D.A. (2006). Regulation of the energy sensor AMP-activated protein kinase by antigen receptor and Ca2+ in T lymphocytes. The Journal of experimental medicine *203*, 1665-1670.

Tanji, T., and Ip, Y.T. (2005). Regulators of the Toll and Imd pathways in the Drosophila innate immune response. Trends in immunology *26*, 193-198.

Tomiyama, H., Matsuda, T., and Takiguchi, M. (2002). Differentiation of human CD8(+) T cells from a memory to memory/effector phenotype. Journal of immunology *168*, 5538-5550.

van der Windt, G.J., Everts, B., Chang, C.H., Curtis, J.D., Freitas, T.C., Amiel, E., Pearce, E.J., and Pearce, E.L. (2012). Mitochondrial respiratory capacity is a critical regulator of CD8+ T cell memory development. Immunity *36*, 68-78.

Vander Heiden, M.G., Cantley, L.C., and Thompson, C.B. (2009). Understanding the Warburg effect: the metabolic requirements of cell proliferation. Science *324*, 1029-1033.

Veiga-Fernandes, H., Walter, U., Bourgeois, C., McLean, A., and Rocha, B. (2000). Response of naive and memory CD8+ T cells to antigen stimulation in vivo. Nature immunology *1*, 47-53.

Wang, R., Dillon, C.P., Shi, L.Z., Milasta, S., Carter, R., Finkelstein, D., McCormick, L.L., Fitzgerald, P., Chi, H., Munger, J., and Green, D.R. (2011). The transcription factor Myc controls metabolic reprogramming upon T lymphocyte activation. Immunity *35*, 871-882.

Warburg, O. (1956). On the Origin of Cancer Cells. Science *123*, 309-314.

Wherry, E.J., Teichgraber, V., Becker, T.C., Masopust, D., Kaech, S.M., Antia, R., von Andrian, U.H., and Ahmed, R. (2003). Lineage relationship and protective immunity of memory CD8 T cell subsets. Nature immunology *4*, 225-234.

Williams, M.A., and Bevan, M.J. (2007). Effector and memory CTL differentiation. Annual review of immunology *25*, 171-192.

Xiao, Z., Casey, K.A., Jameson, S.C., Curtsinger, J.M., and Mescher, M.F. (2009). Programming for CD8 T cell memory development requires IL-12 or type I IFN. Journal of immunology *182*, 2786-2794.

Yi, J.S., Holbrook, B.C., Michalek, R.D., Laniewski, N.G., and Grayson, J.M. (2006). Electron transport complex I is required for CD8+ T cell function. Journal of immunology *177*, 852-862.

Zenhaeusern, G., Gubser, P., Eisele, P., Gasser, O., Steinhuber, A., Trampuz, A., Handschin, C., Luster, A.D., and Hess, C. (2009). A high-mobility, low-cost phenotype defines human effector-memory CD8+ T cells. Blood *113*, 95-99.

Zheng, Y., Collins, S.L., Lutz, M.A., Allen, A.N., Kole, T.P., Zarek, P.E., and Powell, J.D. (2007). A Role for Mammalian Target of Rapamycin in Regulating T Cell Activation versus Anergy. Journal of Immunolgy *178*, 2163-2170.

Zheng, Y., Delgoffe, G.M., Meyer, C.F., Chan, W., and Powell, J.D. (2009). Anergic T cells are metabolically anergic. Journal of immunology *183*, 6095-6101.

ACKNOWLEDGMENTS

Curriculum vitae

Persönliche Angaben

Name	Patrick Gubser
Adresse	St. Johanns-Vorstadt 41
	4056 Basel
Telefonnr.	+41 62 871 53 22
Natelnr.	+41 79 672 08 14
E-mail	patrick_gubser@hotmail.com
Geburtsdatum	16.07.1983
Heimatort	Quarten-Oberterzen (SG)
Zivilstatus	ledig

!

Ausbildung

!

Seit 2010	Doktorat in Medizinisch-biologischer Forschung im Rahmen des schweizerischen MD-PhD Programmes des Schweizerischen Nationalfonds
10/2010	Doktor der Medizin
2003-2009	Medizinstudium an der Universität Basel (Staatsexamen Oktober 2009)
1999–2003	Alte Kantonsschule Aarau, Schwerpunktfach Physik und Anwendungen der Mathematik, Matura (Juli 2003)
1995–1999	Bezirksschule Frick

Arbeitserfahrung

2005-2009	Wissenschaftlicher Mitarbeiter der neurologischen Poliklinik Basel Aktivität: Eingabe von Patientendaten für die GenMSA Studie.
10/2005–07/2007	Assistent für administrative Arbeiten am Training Center für Medizinstudenten (Brain Box)
10/2005–07/2007	Tutor für Physiologie (mit Prof. Dr. U. Otten)
02–03/2006	Aushilfslehrer in Bözen auf Sekundarstufe Aktivität: 5 Wochen Lektionen in Biologie, Deutsch und Sport
10/2006–07/2007	„LAP" Tutor für Medizinstudenten des 1. Jahreskurses: Leukämie und Stammzellen
2006–2007	Handballtrainer des U19 Teams TSV Frick

Wissenschaftliche Arbeiten

6/2013	**Gubser P**, Bantug GR, Razik L, Fischer M, Dimeloe S, Hoenger G, Durovic B, Jauch A and Hess C. Rapid effector memory CD8+ T cell function requires an immediate-early glycolytic switch. (accepted for publication in Nature Immunology)
6/2013	Durovic B, Gasser O, **Gubser P**, Sigle J, Hirsch HH, Stern M, Buser A, Hess C. EBV negativity among individuals older than 60 years is associated with HLA-C and HLA-Bw4 variants, and tonsillectomy. (J Virol.)
5/2013	Mehling M., V. Brinkmann, Burgener AV, **Gubser P**, Luster AD, Kappos L, Hess C. Homing-frequency of human T-cells inferred from peripheral blood depletion-kinetics after S1P-receptor blockade. (Journal of Allergy and Clinical Immunology)
09/2011	Kesten F, Aschwanden M, **Gubser P**, Glatz K, Daikeler T, Hess C. Giant cell arteritis--a changing entity. (Swiss Med Wkly 2011)
10/2008	Zenhaeusern G, **Gubser P,** Eisele P, et al. A "high-mobility low-cost" phenotype defines human effector-memory CD8+ T-cells. (Blood)
06/2003	Maturarbeit: Epigenetische Experimente zur Augenfarbe bei Drosophila melanogaster, ausgezeichnet von der ANG (Aargauische Naturforschende Gesellschaft)

Sprachen

Muttersprache	Deutsch		
	Französisch	8 Jahre	gut
	Englisch	6 Jahre	fliessend
	Latein	6 Jahre	

Militär

Leutnant, Schularzt

Hobbies

Handball, Beach-Volleyball, E-Gitarre, Schwimmen, Börse